Available online at www.sciencedirect.com
SCIENCE DIRECT®
International Journal of Solids and Structures 43 (2006) 2868–2903
INTERNATIONAL JOURNAL OF SOLIDS and STRUCTURES
www.elsevier.com/locate/ijsolstr

Efficient computation of order and mode of three-dimensional stress singularities in linear elasticity by the boundary finite element method

Christian Mittelstedt [a,*], Wilfried Becker [b,1]

[a] Airbus Germany, Kreetslag 10, D-21129 Hamburg, Germany
[b] Department of Mechanics, Darmstadt University of Technology, Hochschulstr. 1, D-64289 Darmstadt, Germany

Received 19 October 2004; received in revised form 22 May 2005
Available online 28 February 2006

Abstract

The Boundary Finite Element Method (BFEM), a novel semi-analytical boundary element procedure solely relying on standard finite element formulations, is employed for the investigation of the orders and modes of three-dimensional stress singularities which occur at notches and cracks in isotropic halfspaces as well as at free edges and free corners of layered plates. After a comprehensive literature review and a concise introduction to the standard three-dimensional BFEM formulation for the static analysis of general unbounded structures, we demonstrate the application of the BFEM for the computation of the orders and modes of two-dimensional and three-dimensional stress singularities for several classes of problems within the framework of linear elasticity. Special emphasis is placed upon the investigation of stress concentration phenomena as they occur at straight free edges and at free corners of arbitrary opening angles in composite laminates. In all cases, the BFEM computations agree excellently with available reference results. The required computational effort is found to be considerably lower compared to e.g. standard Finite Element Method (FEM) computations. In the case of free laminate corners, numerous new results on the occurring stress singularities are presented. It is found that free-corner problems generally seem to involve a more pronounced criticality than the corresponding free-edge situations.

Keywords: Composites; Laminates; Boundary finite element method; Stress concentrations; Stress singularities; Notches; Cracks; Free-edge effect; Free-corner effect

1. Introduction

Fiber-reinforced laminated structures under thermomechanical loading conditions (so-called laminates, Fig. 1) may exhibit severe singular interlaminar stress concentrations in the vicinity of geometrical and/or physical discontinuities. A well-known example of this class of elasticity problems is the classical free-edge

* Corresponding author. Tel.: +49 40 74370.
E-mail addresses: christian.mittelstedt@airbus.com (C. Mittelstedt), becker@mechanik.tu-darmstadt.de (W. Becker).
[1] Tel.: +49 6151 16 3174; fax: +49 6151 16 6117.

0020-7683/$ - see front matter © 2005 Published by Elsevier Ltd.
doi:10.1016/j.ijsolstr.2005.05.059

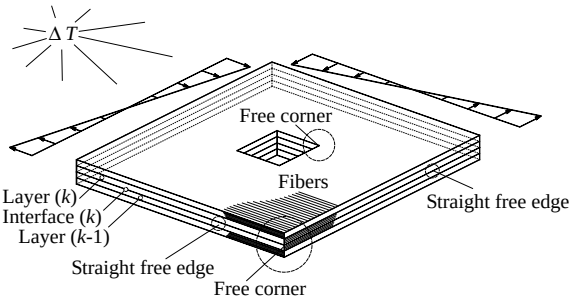

Fig. 1. Laminate under thermomechanical load, potential locations for stress concentrations.

effect (see e.g. Herakovich, 1989a; Kant and Swaminathan, 2000 or Mittelstedt and Becker, 2004a) which has been the subject of thorough investigations especially since the pioneering work of Pipes and Pagano in 1970. Free-edge stress fields are of a singular three-dimensional nature at the interfaces of dissimilar layers in the vicinity of straight free edges of a laminate. Such interlaminar stress concentration phenomena are mainly evoked by the discontinuous change of the material properties at the interfaces between two dissimilar laminate layers. Being highly localized, interlaminar stresses rapidly decay until in the inner laminate regions the assumptions of Classical Laminate Plate Theory (CLPT, see e.g. Herakovich, 1998 or Reddy, 2004) entirely hold and only inplane stresses remain.

An exact elasticity solution for the free-edge problem is unknown. Since a thorough understanding of free-edge stress phenomena and their appropriate analysis have a high practical importance due to the possible onset and propagation of delaminations as a consequence of free-edge stress concentrations, there is a considerable number of works available concerning the numerical treatment of such stress concentration problems as well as on the development of approximate closed-form approaches based on various modeling conceptions. Early numerical approaches towards the assessment of free-edge stress concentrations were performed by e.g. Pipes and Pagano (1970), Pipes (1980), Altus et al. (1980) and Bauld et al. (1985) employing the Finite Difference Method (FDM). However, beside the application of the FDM there are also some very early works available in which Finite Element Method (FEM) formulations were employed, see e.g. the investigations of Isakson/Levy or Rybicki, both from 1971. Mainly, FEM approaches to free-edge effects may be subdivided into investigations in which standard displacement based finite elements are employed as they are also commonly available in commercial FEM program codes (see e.g. the works of Wang and Crossman, 1977; Whitcomb et al., 1982; Rohwer, 1982; Whitcomb and Raju, 1983; Wu, 1987; Ye, 1990; Lessard et al., 1996; Lindemann and Becker, 2002a or Artel and Becker, in press) and such approaches where especially adapted FEM formulations are used (see e.g. Spilker, 1980; Spilker and Chou, 1980; Wang and Yuan, 1983a,b; Gruttmann and Wagner, 1994; Robbins and Reddy, 1996; Gaudenzi et al., 1998 or Mannini and Gaudenzi, 2003). However, beside the well known standard methodologies FDM and FEM, the employment of other numerical approaches has been reported as well: Öry et al. (1984) have used the method of transfer matrices whereas Davi (1996) has employed a Boundary Element Method (BEM) formulation. Furthermore, Lindemann and Becker (2000, 2002b) have employed an especially adjusted Boundary Finite Element Method (BFEM) formulation for the computation of free-edge stress fields. Since the BFEM is also the method of choice for all asymptotic computations in the present paper, we will present the basics of this quite novel method at some length in a subsequent section. Concerning approximate closed-form analysis methods for free-edge effects, we may roughly subdivide the available investigations into such approaches which are based on stress shape assumptions and those which employ adequate formulations for the displacement field, wherein mixed formulations are also possible. A further classification of closed-form approaches can be identified by sorting the available publications into such investigations which employ layerwise formulations and such approaches where formulations are used which are valid through the complete laminate thickness. Mixed forms, however, are also possible within this classification. Displacement based approaches that employ formulations through the complete laminate thickness are available with the works of e.g. Pagano (1974), Krishna Murty and Hari Kumar (1989) and Becker (1993, 1994) while e.g. Pipes and Pagano (1974), Hsu and Herakovich (1977), Zhu and Lam (1998) and Tahani and Nosier (2003) have applied layerwise

displacement formulations. Puppo and Evensen (1970), Tang (1975), Pagano (1978a,b), Kassapoglou and Lagace (1986), Rose and Herakovich (1993), Yin (1994), Kim and Atluri (1994) and Cho and Kim (2000) have employed stress based layerwise approaches for their investigations on free-edge effects, among others. Experimental evidence for the existence of severe free-edge stress fields and the possible hazard of interlaminar failure modes as a result of interlaminar stress concentrations has been given by e.g. Pipes and Daniel (1971), Whitney and Browning (1972), Herakovich et al. (1985), Herakovich (1989a,b), Kim (1989) and Whitney (1989). Since the stress field in the vicinity of edge interfaces between dissimilar laminate layers is dominated by a mathematical singularity, there is also a multitude of investigations available in which the asymptotical behaviour of the state variables near free interface edges is considered. Raju and Crews (1981), Ting and Chou (1981), Wang and Choi (1982a,b), Zwiers et al. (1982), Delale (1984), Yeh and Tadjbakhsh (1986), Stolarski and Chiang (1989), Ding and Kumosa (1994), Gu and Belytschko (1994), Zhong (1994), Kim and Im (1995a,b), Seweryn and Molski (1996), Li et al. (2001), Li and Recho (2002) or Li (2002) have addressed this topic, among others.

Even though free-edge effects are fairly well understood, the occurring stress concentrations in the vicinity of free laminate corners (so-called free-corner effect) where two free edges intersect under an arbitrary corner angle have escaped broader attention of the scientific community so far. In the light of the overwhelming number of scientific investigations on free-edge effects which have been published throughout a time period of more than the last 30 years this is all the more puzzling, especially since there have been early works that gave some first hints on possibly critical free-corner stress fields: As an example, in an older numerical work Griffin (1988) presented three-dimensional FEM results for stress fields in the vicinity of rectangular angle-ply laminate corners and has shown that free-corner effects may be the cause for severe three-dimensional interlaminar stress fields which clearly exceed the corresponding interlaminar free-edge stress peaks. It is easy to comprehend that analogously to the free-edge effect severe stress concentrations of a three-dimensional and singular character also occur at free laminate corners so that the finding of answers to the question "*What exactly happens near a free laminate corner?*" should be the topic of future investigations.

The occurrence of three-dimensional and possibly singular stress fields in the vicinity of free laminate corners has been given significant experimental evidence, e.g. in a recent work of Herrmann and Linnenbrock (2002). Because displacements and stresses in the vicinity of a free laminate corner are dependent on all three coordinate directions, especially the development of approximate closed-form analysis methods is a quite difficult task. In addition, this also holds true for numerical analyses, e.g. with standard FEM formulations, since for the sufficiently accurate analysis of free-corner stress fields with involved corner singularities a high degree of mesh refinement is necessary in the closer corner regions. This need for discretization refinements may easily exceed available computational resources and renders this class of methods generally unsuitable for the performance of optimization procedures or extensive parameter studies. Hence, it is of special interest to develop alternative analysis methods which deliver results with acceptable accuracy yet reasonable computational effort. Some closed-form analytical works on free-corner effects have been developed throughout the last years. Becker et al. (1999) investigated the interlaminar stress field in the vicinity of rectangular corners of cross-ply laminates under thermal load and assumed a layerwise stress field in the form of simple inplane exponential terms and polynomials through the thickness. Free parameters in the stress representations were determined from the principle of minimum complementary energy. The method yields results with reasonable accuracy and without significant computational effort, yet it neglects the full three-dimensional dependence of the inplane normal stresses and is restricted to pure cross-ply layups. In order to improve this methodology, Mittelstedt and Becker (2003a, 2004b) used an upgraded inplane stress field for laminates with arbitrary non-orthotropic layups. Mittelstedt and Becker (2003b) introduced a simple displacement based approach for pure rectangular cross-ply layups under thermal load by using a higher order single layer theory with trigonometric terms through the complete laminate thickness. Furthermore, Mittelstedt and Becker (2004c,d) employed a layerwise displacement based approach which applies a discretization of symmetric laminates with isotropic layers and cross-ply plates into an arbitrary number of mathematical layers through the plate thickness. Therein, the displacement field is formulated with a linear interpolation scheme through the layer thickness and unknown functions with respect to the inplane coordinates, the latter of which are eventually determined by the principle of minimum potential energy of the laminate. However, even though approximate analysis methods may prove valuable for the assessment of three-dimensional fields in the vicinity of free laminate

corners, in general such methods are not easy to derive and are usually restricted to very special cases of application. Thus, in order to overcome this limitation some authors have also conducted numerical investigations concerning corner problems in laminate elasticity, among them Griffin (1988), Icardi and Bertetto (1995) and Herrmann and Linnenbrock (2002), mainly with the help of FEM formulations. Note that there is an impressive number of investigations available which are concerned with the two-dimensional asymptotical behaviour of the elastic state variables in the near field of free interface edges. However, the list of available publications becomes significantly shorter when results are sought on three-dimensional corner stress singularities. Nevertheless, this fundamental problem has been dealt with occasionally in some more recent works. Koguchi (1997) used a boundary element approach with quadrilateral serendipity elements and addressed the stress state at three-dimensional vertices of joints between two dissimilar isotropic materials. Koguchi applied mesh refinements in the interface region and determined the order of the stress singularity by a curve fitting technique. Labossiere and Dunn (2001) employed a FEM eigenanalysis method for the computation of orders and modes of stress singularities and correlated the crack initiation at three-dimensional bimaterial interface corners with critical values of the intensities of the occurring singular stress fields. Using an analogous FEM eigenanalysis approach, Dimitrov et al. (2001, 2002) presented results for three-dimensional stress singularities near free laminate corners and for several other elasticity problems involving three-dimensional stress singularities.

The analysis of singular elasticity problems by means of purely numerical analysis tools is usually expensive in a computational sense, hence there is a particular interest in introducing new and efficient analysis methods like e.g. the Boundary Finite Element Method (BFEM, see e.g. Wolf and Song, 1996a or Wolf, 2003), especially when detailed information on the asymptotical behaviour of the state variables—displacements, strains and stresses—in the vicinity of a three-dimensional free laminate corner is sought. The BFEM has been originally developed by Wolf and Song (1996a) for the numerical investigation of unbounded structures in the framework of time-dependent soil mechanics. Since it is felt that the BFEM has not yet achieved the attention it deserves as an efficient analysis tool also in the framework of laminate elasticity, we will give a concise summary of the general theoretical background of the BFEM for the case of a *static analysis of a linear elastic unbounded structure*. The general dynamic case as well as a good number of examples of applications can be found in full detail in the book by Wolf and Song (1996a). In the focal part of this work we will demonstrate the efficient applicability of the BFEM to the computation of the orders and modes of the occurring stress singularities in three-dimensional notch and crack situations as well as in the vicinity of free edges and corners of composite laminates with arbitrary non-orthotropic lamination schemes. Therein, emphasis will be put on the latter edge and corner situations in composite laminates for which numerous new results are presented and for which there is still a significant backlog concerning the detailed knowledge of the asymptotical behaviour of the involved field quantities.

The employment of the BFEM for a good variety of analysis purposes has been reported by the original authors in a series of papers. Song and Wolf (1995a) considered the case of two-dimensional wave propagation, and the BFEM formulation for the scalar wave equation was derived. Wolf and Song (1996b) investigated three-dimensional wave propagation problems also. Two-dimensional and three-dimensional wave propagation problems were adressed by Wolf and Song (1995) and Song and Wolf (1995b), respectively, wherein the formulations for the compressible vector wave equation were derived. The topic of diffusion was considered in Song and Wolf (1996). In Song and Wolf (1997), Song and Wolf (1998a) and Wolf and Song (1998a), beside several other relevant engineering problems, examples for the computation of generalized stress intensity factors and orders of singularities within the framework of fracture mechanics were considered. Additionally, the derivation of the method was not mechanically based as in the foregoing works (where the method was denoted *consistent infinitesimal finite element cell method* due to its derivation based on finite element formulations) but was derived starting from the governing partial differential equations. A transformation from the cartesian coordinate system to the scaled boundary coordinates (i.e. a radial and two circumferential coordinates) and the application of a weighted residuals technique finally yielded ordinary differential equations in the radial direction which were solved in a closed-form analytical way. Applying this derivation of the method and extending the paper of Song and Wolf (1997), in Wolf and Song (1998b) and Song and Wolf (1998b) a formulation for the displacement unit-impulse response and an analytical solution of the scaled boundary finite element equation in the frequency domain were given and several problems

including unbounded and bounded media were solved. In Song and Wolf (1999a) the diffusion problem was revisited. Nonvanishing body loads were incorporated into the method formulation in Song and Wolf (1999b). Basic examples and derivations for simple wave propagation problems were given in the tutorial papers Wolf and Song (2000) and Song and Wolf (2000). Furthermore, both possibilities of derivation of the method were illustrated in Wolf and Song (2000). The papers of Song and Wolf (2001a) and Song and Wolf (2002) dealt with topics of linear fracture mechanics. The possibilities of substructuring in the course of the BFEM and the usage of domains discretized by the BFEM as superelements for subsequent analyses with the standard FEM were also addressed. Methods for stress recovery and error estimation as well as hierarchical adaptive *h*-methods for the BFEM were discussed in Deeks and Wolf (2002a,b), whereas Deeks and Wolf (2002c) also presented a derivation of the BFEM based on virtual work. Comprehensive survey papers are available with Song and Wolf (2001b) and Wolf and Song (2002). The BFEM has also been reported to be successfully implemented for several problems in laminate elasticity, see e.g. Lindemann and Becker (2000, 2002b), Müller et al. (in press) or Wigger and Becker (2004). The theoretical backgrounds of the BFEM for novel aspects of application like e.g. electromagnetics have been given by Prasanna Rajan and Raju (2002a,b). The origins of the BFEM can be traced back, e.g. to a pioneering paper by Dasgupta (1982) who presented the so-called cloning algorithm for the determination of the dynamic stiffness matrix of an unbounded continuum. Dasgupta used the average value of the two characteristic lengths of the two similar boundaries of the finite element cell when formulating the similarity-based relationship and computed the dynamic stiffness matrix of the unbounded continuum from an eigenvalue problem. Some historical notes on the development of the BFEM can also be found in Wolf and Song (1996a) and Wolf (2003).

2. The boundary finite element method (BFEM)

2.1. Basic concept

The BFEM can be characterized as a fundamental-solution-less BEM solely based on finite elements appropriate for the investigation of bounded as well as unbounded structures. As a prerequisite the BFEM assumes a certain scalability of the given structure with respect to a discrete point, the so-called similarity center S. Consider the unbounded or semi-infinite layered structure with an irregular boundary as given in Fig. 2, left portion, and let us for the explanation of the basic concepts of the BFEM refer to a three-dimensional structure with the boundary at the characteristic radial distance r_i, measured with respect to the similarity center S. The unbounded structure (Fig. 2, left portion), denoted as Ω_i, includes the boundary Γ_i (also: inner or interior boundary). Let us introduce a second artificial boundary Γ_e (outer or exterior boundary) at some distance from Γ_i and with the characteristic radial distance r_e (Fig. 2, right portion) measured from the similarity center S. This exterior boundary Γ_e is similar to the original boundary Γ_i in the sense that we may describe Γ_e by a centric scaling of the coordinates of Γ_i with respect to the similarity center S, i.e. we have $r_\mathrm{e} = (1 + w)r_\mathrm{i}$. Herein, w is a dimensionless scaling parameter. The unbounded structure in the range $r \geqslant r_\mathrm{e}$ bounded by Γ_e is denoted as Ω_e. The resultant space between Γ_i and Γ_e (so-called finite element

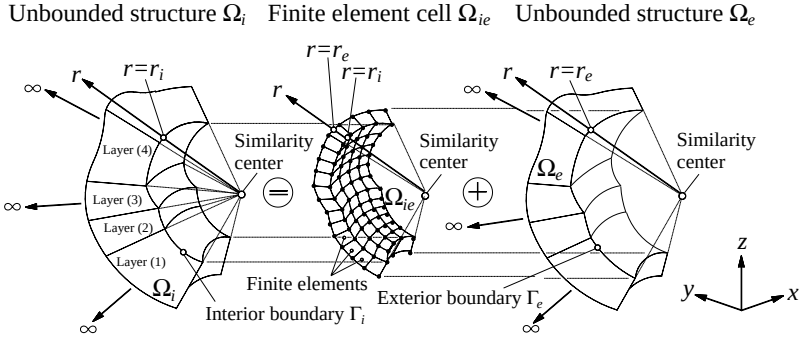

Fig. 2. Principle of scalability and discretization of an infinite three-dimensional layered structure.

cell), denoted as Ω_{ie} and enclosed in the characteristic interval $r_i \leqslant r \leqslant r_e$, is discretized with one single layer of standard displacement based isoparametric finite volume elements (Fig. 2, middle portion) the nodal arrangements of which must satisfy scalability as well, i.e. the finite elements have a linear interpolation scheme in the radial direction and arbitrary nodal arrangements in the two circumferential directions which nevertheless have to be identical on both boundaries (see Fig. 3 where a three-dimensional element with the natural coordinates ξ, η, ζ and the corresponding master element for the interpolation scheme on the boundaries is given). Presently, the employed elements are supposed to be 16-noded volume elements with 8 nodes on both boundaries Γ_i and Γ_e. Note that the remaining structure Ω_e which is bounded by the similar exterior boundary Γ_e at the characteristic distance r_e is not discretized. Note also that straight crack faces or interfaces between dissimilar materials passing through the similarity center do not have to be discretized as well.

The basic and essential features of the BFEM are as follows. First, if we assemble the finite element cell Ω_{ie} and the structure Ω_e, the original unbounded structure Ω_i with the boundary Γ_i at the characteristic radial distance r_i is recovered. Analogously, the unknown stiffness matrices of the two similar unbounded structures Ω_i and Ω_e, respectively can be related. From assembling the unknown stiffness matrix of Ω_e and the stiffness matrix of the finite element cell Ω_{ie}, the unknown stiffness matrix of Ω_i can be determined. Since the stiffness properties of the finite element cell Ω_{ie} can be concluded from the employed discretization scheme, the stiffness matrix of the discretized finite element cell Ω_{ie} can be considered as known a priori. Second, by taking the introduced similarity of the two unbounded structures Ω_i and Ω_e into account, a second relation between the two unknown stiffness matrices of Ω_i and Ω_e is easily established. Hence, we postulate two relations between the stiffness properties of Ω_i and Ω_e, one relation based on assemblage and equilibrium and the other relation based on similarity. This will finally enable us to express the stiffness properties of Ω_i in terms of the stiffness properties of the finite element cell Ω_{ie} which follow from well-known and established FEM relations. The resultant formulations will then only depend on the geometry of Γ_i, on the material properties of Ω_i and on the employed FEM discretization of the finite element cell Ω_{ie}. The employment of both relations finally leads to an algebraic matrix Riccati equation which governs the unknown boundary stiffness matrix. This equation can also be written in terms of an equivalent eigenvalue problem from which a system of first order differential equations with respect to the radial direction can be derived for the displacement components. This system of differential equations can be solved in a closed-form analytical manner. The resultant BFEM procedure is thus exact in the radial direction and in the circumferential directions converges in the FEM sense, i.e. it relies on the employed shape functions. Hence, the BFEM uses a weak formulation in the circumferential directions but a strong formulation with respect to the radial coordinate and it is appropriate to speak of a method which combines specific advantages of the BEM and the standard FEM. Representations for strains and stresses can finally be derived in a straightforward way. Since no fundamental solution is required, anisotropic material behaviour can be incorporated into the formulations without principal difficulties. The reader should note that the BFEM is a discrete version of continuous methods which have been presented in several forms since 1961: to name some examples, let us cite, e.g. Abramov (1961) (transfer of boundary conditions), Haskell (1964) (propagator in time harmonic elasticity), Bellman et al. (1967) (invariant embedding), Bossavit and Fremond (1976) (frontal method), Bui (1994) (transfer matrix of operators for Cauchy problems) or Zhong (1994) (Hamiltonian method).

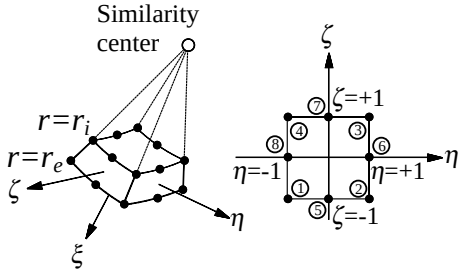

Fig. 3. Three-dimensional 16-noded volume element (left), two-dimensional master element (right).

2.2. BFEM formulation

We will derive the array $\underline{N} = \underline{N}(\xi,\eta,\zeta)$ of shape functions of a three-dimensional 16-noded volume master element (Fig. 3, left portion) from the array of the shape functions $\underline{N} = \underline{N}(\eta,\zeta)$ of the two-dimensional 8-noded surface master element (Fig. 3, right portion) which presently reads:

$$\underline{N}(\eta,\zeta) = (\,N_1(\eta,\zeta) \quad N_2(\eta,\zeta) \quad N_3(\eta,\zeta) \quad N_4(\eta,\zeta) \quad N_5(\eta,\zeta) \quad N_6(\eta,\zeta) \quad N_7(\eta,\zeta) \quad N_8(\eta,\zeta)\,)^{\mathrm{T}}. \tag{1}$$

For convenience we will use a decomposed notation for $\underline{N}(\xi,\eta,\zeta)$ using the two subarrays $\underline{N}_{\mathrm{i}}(\xi,\eta,\zeta)$ and $\underline{N}_{\mathrm{e}}(\xi,\eta,\zeta)$ which correspond to the interior boundary Γ_{i} and the exterior boundary Γ_{e}, respectively:

$$\underline{N}(\xi,\eta,\zeta) = (\,\underline{N}_{\mathrm{i}}(\xi,\eta,\zeta) \quad \underline{N}_{\mathrm{e}}(\xi,\eta,\zeta)\,)^{\mathrm{T}}. \tag{2}$$

Let us introduce the radial coordinate ξ_j with $j = \mathrm{i}, \mathrm{e}$, where $\xi_{\mathrm{i}} = -1$ at the interior boundary and $\xi_{\mathrm{e}} = +1$ at the exterior boundary hold. We may then use a contracted notation for the array of shape functions of the three-dimensional master element on the boundary Γ_j:

$$\underline{N}_j(\xi,\eta,\zeta) = \frac{1}{2}(1+\xi_j\xi)\underline{N}(\eta,\zeta). \tag{3}$$

With respect to an arbitrary node k on the boundary Γ_j, the shape function $N_{jk}(\xi,\eta,\zeta)$ of the full three-dimensional element then reads (with $j = \mathrm{i}, \mathrm{e}$ and presently $k = 1,2,\ldots,8$):

$$N_{jk}(\xi,\eta,\zeta) = \frac{1}{2}(1+\xi_j\xi)N_k(\eta,\zeta). \tag{4}$$

Note that this scheme of shape functions means a simple linear dependence of the displacements on the radial coordinate. Since we refer to problems which obey similarity, we may write the cartesian coordinates $\underline{x}_{\mathrm{e}}$, $\underline{y}_{\mathrm{e}}$, $\underline{z}_{\mathrm{e}}$ of the nodes on the exterior boundary Γ_{e} in terms of the coordinates $\underline{x}$, $\underline{y}$, $\underline{z}$ of the nodes on the interior boundary Γ_{i} in analogy to the radial coordinate as

$$\underline{x}_{\mathrm{e}} = (1+w)\underline{x}, \quad \underline{y}_{\mathrm{e}} = (1+w)\underline{y}, \quad \underline{z}_{\mathrm{e}} = (1+w)\underline{z}. \tag{5}$$

We have omitted the index i for the interior boundary at this point since in the course of a practical application of the BFEM only this boundary is discretized as will be shown further on. According to the isoparametric mapping rule, the coordinates x, y, z of a point within the three-dimensional finite element can be written in terms of the nodal coordinates of the surface elements on Γ_{i} and the employed shape functions. This eventually leads to the following formulations:

$$x = \left(1+\frac{w}{2}(1+\xi)\right)\underline{N}^{\mathrm{T}}(\eta,\zeta)\underline{x}, \quad y = \left(1+\frac{w}{2}(1+\xi)\right)\underline{N}^{\mathrm{T}}(\eta,\zeta)\underline{y}, \quad z = \left(1+\frac{w}{2}(1+\xi)\right)\underline{N}^{\mathrm{T}}(\eta,\zeta)\underline{z}. \tag{6}$$

The relation between the partial derivatives of the shape function of the node k on the boundary Γ_j in local element coordinates ξ, η, ζ and in global coordinates x, y, z can be written by introducing the Jacobian matrix $\underline{\underline{J}}$:

$$\begin{pmatrix} N_{jk,\xi}(\xi,\eta,\zeta) \\ N_{jk,\eta}(\xi,\eta,\zeta) \\ N_{jk,\zeta}(\xi,\eta,\zeta) \end{pmatrix} = \begin{bmatrix} x_{,\xi} & y_{,\xi} & z_{,\xi} \\ x_{,\eta} & y_{,\eta} & z_{,\eta} \\ x_{,\zeta} & y_{,\zeta} & z_{,\zeta} \end{bmatrix} \begin{pmatrix} N_{jk,x}(\xi,\eta,\zeta) \\ N_{jk,y}(\xi,\eta,\zeta) \\ N_{jk,z}(\xi,\eta,\zeta) \end{pmatrix} = \underline{\underline{J}} \begin{pmatrix} N_{jk,x}(\xi,\eta,\zeta) \\ N_{jk,y}(\xi,\eta,\zeta) \\ N_{jk,z}(\xi,\eta,\zeta) \end{pmatrix}. \tag{7}$$

Therein, an index behind a comma denotes a derivative with respect to the corresponding coordinate. The derivatives of the shape function $N_{jk}(\xi,\eta,\zeta)$ of the node k on the boundary Γ_j in global coordinates then eventually can be shown to read:

$$\begin{pmatrix} N_{jk,x}(\xi,\eta,\zeta) \\ N_{jk,y}(\xi,\eta,\zeta) \\ N_{jk,z}(\xi,\eta,\zeta) \end{pmatrix} = \frac{\xi_j}{w} \begin{pmatrix} j_{11} \\ j_{21} \\ j_{31} \end{pmatrix} N_k(\eta,\zeta) + \frac{1+\xi_j\xi}{2\left(1+\frac{w}{2}(1+\xi)\right)} \left[\begin{pmatrix} j_{12} \\ j_{22} \\ j_{32} \end{pmatrix} N_{k,\eta}(\eta,\zeta) + \begin{pmatrix} j_{13} \\ j_{23} \\ j_{33} \end{pmatrix} N_{k,\zeta}(\eta,\zeta) \right]. \tag{8}$$

Therein, the components j_{ij} result by the inversion of the Jacobian matrix $\underline{\underline{J}}$ and will not be given in detail due to their lengthy nature. In the framework of a geometrically linear theory, the relation between the

displacements and the components of the infinitesimal strain tensor is conveniently written by means of the operator matrix $\underline{\underline{B}}_{jk}$ for the node k on the boundary Γ_j:

$$\underline{\underline{B}}_{jk} = \begin{bmatrix} N_{jk,x}(\xi,\eta,\zeta) & 0 & 0 \\ 0 & N_{jk,y}(\xi,\eta,\zeta) & 0 \\ 0 & 0 & N_{jk,z}(\xi,\eta,\zeta) \\ 0 & N_{jk,z}(\xi,\eta,\zeta) & N_{jk,y}(\xi,\eta,\zeta) \\ N_{jk,z}(\xi,\eta,\zeta) & 0 & N_{jk,x}(\xi,\eta,\zeta) \\ N_{jk,y}(\xi,\eta,\zeta) & N_{jk,x}(\xi,\eta,\zeta) & 0 \end{bmatrix} = \frac{\xi_j}{w}\underline{\underline{B}}^1_k + \frac{1+\xi_j\xi}{2\left(1+\frac{w}{2}(1+\xi)\right)}\underline{\underline{B}}^2_k. \tag{9}$$

Therein, we have introduced the abbreviations

$$\underline{\underline{B}}^1_k = \begin{bmatrix} j_{11} & 0 & 0 \\ 0 & j_{21} & 0 \\ 0 & 0 & j_{31} \\ 0 & j_{31} & j_{21} \\ j_{31} & 0 & j_{11} \\ j_{21} & j_{11} & 0 \end{bmatrix} N_k(\eta,\zeta), \quad \underline{\underline{B}}^2_k = \begin{bmatrix} j_{12} & 0 & 0 \\ 0 & j_{22} & 0 \\ 0 & 0 & j_{32} \\ 0 & j_{32} & j_{22} \\ j_{32} & 0 & j_{12} \\ j_{22} & j_{12} & 0 \end{bmatrix} N_{k,\eta}(\eta,\zeta) + \begin{bmatrix} j_{13} & 0 & 0 \\ 0 & j_{23} & 0 \\ 0 & 0 & j_{33} \\ 0 & j_{33} & j_{23} \\ j_{33} & 0 & j_{13} \\ j_{23} & j_{13} & 0 \end{bmatrix} N_{k,\zeta}(\eta,\zeta). \tag{10}$$

Note that $\underline{\underline{B}}^1_k$ and $\underline{\underline{B}}^2_k$ are not functions of ξ and thus are identical for both boundaries Γ_i and Γ_e. It is convenient to assemble the matrices $\underline{\underline{B}}^1_k$ and $\underline{\underline{B}}^2_k$ of all n_e nodes on the boundary Γ_j and to compile them in the matrices $\underline{\underline{B}}^1$ and $\underline{\underline{B}}^2$ which again are not functions of ξ:

$$\underline{\underline{B}}^1 = \begin{bmatrix} \underline{\underline{B}}^1_1 & \underline{\underline{B}}^1_2 & \cdots & \underline{\underline{B}}^1_k & \cdots & \underline{\underline{B}}^1_{n_\mathrm{e}} \end{bmatrix}, \quad \underline{\underline{B}}^2 = \begin{bmatrix} \underline{\underline{B}}^2_1 & \underline{\underline{B}}^2_2 & \cdots & \underline{\underline{B}}^2_k & \cdots & \underline{\underline{B}}^2_{n_\mathrm{e}} \end{bmatrix}. \tag{11}$$

The operator matrix $\underline{\underline{B}}_j$ of the boundary Γ_j reads:

$$\underline{\underline{B}}_j = \frac{\xi_j}{w}\underline{\underline{B}}^1 + \frac{1+\xi_j\xi}{2\left(1+\frac{w}{2}(1+\xi)\right)}\underline{\underline{B}}^2. \tag{12}$$

This corresponds to the decomposition of the operator matrix $\underline{\underline{B}}$ of the three-dimensional finite element with respect to the two boundaries Γ_i and Γ_e, hence we have:

$$\underline{\underline{B}} = \begin{bmatrix} \underline{\underline{B}}_\mathrm{i} & \underline{\underline{B}}_\mathrm{e} \end{bmatrix}. \tag{13}$$

Let us now refer to the standard FEM formulation for the stiffness matrix $\underline{\underline{K}}$ of a three-dimensional finite element which requires integration over the element volume V as follows:

$$\underline{\underline{K}} = \int\int\int_V \underline{\underline{B}}^\mathrm{T}\underline{\underline{C}}\underline{\underline{B}}\,\mathrm{d}V. \tag{14}$$

The symmetric matrix $\underline{\underline{C}}$ contains the elastic stiffness components $C_{mn} = C_{nm}$ of the considered material. Hooke's generalized law $\underline{\sigma} = \underline{\underline{C}}\underline{\varepsilon}$ in the case of three-dimensional on-axis orthotropy reads:

$$\begin{pmatrix} \sigma_{xx} \\ \sigma_{yy} \\ \sigma_{zz} \\ \sigma_{yz} \\ \sigma_{xz} \\ \sigma_{xy} \end{pmatrix} = \begin{bmatrix} C_{11} & C_{12} & C_{13} & 0 & 0 & 0 \\ C_{21} & C_{22} & C_{23} & 0 & 0 & 0 \\ C_{31} & C_{32} & C_{33} & 0 & 0 & 0 \\ 0 & 0 & 0 & C_{44} & 0 & 0 \\ 0 & 0 & 0 & 0 & C_{55} & 0 \\ 0 & 0 & 0 & 0 & 0 & C_{66} \end{bmatrix} \begin{pmatrix} \varepsilon_{xx} \\ \varepsilon_{yy} \\ \varepsilon_{zz} \\ \gamma_{yz} \\ \gamma_{xz} \\ \gamma_{xy} \end{pmatrix}. \tag{15}$$

Herein, we have assembled the normal stresses σ_{xx}, σ_{yy}, σ_{zz} and the shear stresses σ_{yz}, σ_{xz}, σ_{xy} in the one-dimensional array $\underline{\sigma}$, the normal strains ε_{xx}, ε_{yy}, ε_{zz} and the shear strains γ_{yz}, γ_{xz}, γ_{xy} are compiled analogously in the one-dimensional array $\underline{\varepsilon}$. In a composite laminate the individual layers can have an arbitrary inplane material orientation angle θ with respect to the global laminate coordinates. Let us thus consider a rotation

θ of the material axes about the global z-axis, wherein the rotated $\bar{x}$ and $\bar{y}$-axes remain orthogonal to each other. The elastic stiffness components $\bar{C}_{mn}$ in an off-axis system $\bar{x}$, $\bar{y}$, $\bar{z}$ (with the rotation angle θ between the axes x and $\bar{x}/y$ and $\bar{y}$) then have to be transformed from the values C_{mn} as given in the on-axis system. The according transformation rules can be derived by means of elementary tensor transformations and are given as

$$\begin{aligned}
\bar{C}_{11} &= C_{11}\cos^4\theta + C_{22}\sin^4\theta + 2C_{12}\cos^2\theta\sin^2\theta + 4C_{66}\cos^2\theta\sin^2\theta,\\
\bar{C}_{22} &= C_{11}\sin^4\theta + C_{22}\cos^4\theta + 2C_{12}\cos^2\theta\sin^2\theta + 4C_{66}\cos^2\theta\sin^2\theta,\\
\bar{C}_{33} &= C_{33}, \quad \bar{C}_{44} = C_{44}\cos^2\theta + C_{55}\sin^2\theta, \quad \bar{C}_{55} = C_{44}\sin^2\theta + C_{55}\cos^2\theta,\\
\bar{C}_{66} &= (C_{11} + C_{22} - 2C_{12})\cos^2\theta\sin^2\theta + C_{66}(\cos^2\theta - \sin^2\theta)^2,\\
\bar{C}_{12} &= (C_{11} + C_{22} - 4C_{66})\cos^2\theta\sin^2\theta + C_{12}(\cos^4\theta + \sin^4\theta),\\
\bar{C}_{13} &= C_{13}\cos^2\theta + C_{23}\sin^2\theta, \quad \bar{C}_{23} = C_{13}\sin^2\theta + C_{23}\cos^2\theta,\\
\bar{C}_{16} &= (C_{11}\cos^2\theta - C_{22}\sin^2\theta)\cos\theta\sin\theta + (C_{12} + 2C_{66})(\cos\theta\sin^3\theta - \cos^3\theta\sin\theta),\\
\bar{C}_{26} &= (C_{11}\sin^2\theta - C_{22}\cos^2\theta)\cos\theta\sin\theta + (C_{12} + 2C_{66})(\cos^3\theta\sin\theta - \cos\theta\sin^3\theta),\\
\bar{C}_{36} &= (C_{13} - C_{23})\cos\theta\sin\theta, \quad \bar{C}_{45} = (C_{55} - C_{44})\cos\theta\sin\theta.
\end{aligned} \tag{16}$$

Hooke's generalized law in the off-axis system $\bar{x}$, $\bar{y}$, $\bar{z}$ then becomes:

$$\begin{pmatrix} \sigma_{xx}\\ \sigma_{yy}\\ \sigma_{zz}\\ \sigma_{yz}\\ \sigma_{xz}\\ \sigma_{xy} \end{pmatrix} = \begin{bmatrix} \bar{C}_{11} & \bar{C}_{12} & \bar{C}_{13} & 0 & 0 & \bar{C}_{16}\\ \bar{C}_{21} & \bar{C}_{22} & \bar{C}_{23} & 0 & 0 & \bar{C}_{26}\\ \bar{C}_{31} & \bar{C}_{32} & \bar{C}_{33} & 0 & 0 & \bar{C}_{36}\\ 0 & 0 & 0 & \bar{C}_{44} & \bar{C}_{45} & 0\\ 0 & 0 & 0 & \bar{C}_{54} & \bar{C}_{55} & 0\\ \bar{C}_{61} & \bar{C}_{62} & \bar{C}_{63} & 0 & 0 & \bar{C}_{66} \end{bmatrix} \begin{pmatrix} \varepsilon_{xx}\\ \varepsilon_{yy}\\ \varepsilon_{zz}\\ \gamma_{yz}\\ \gamma_{xz}\\ \gamma_{xy} \end{pmatrix}. \tag{17}$$

The stiffness matrix $\underline{\underline{K}}$ (14) of the three-dimensional finite element is now consequently decomposed into submatrices $\underline{\underline{K}}_{jl}$ concerning the interior boundary Γ_{i} and the exterior boundary Γ_{e} as

$$\underline{\underline{K}} = \begin{pmatrix} \underline{\underline{K}}_{\mathrm{ii}} & \underline{\underline{K}}_{\mathrm{ie}}\\ \underline{\underline{K}}_{\mathrm{ei}} & \underline{\underline{K}}_{\mathrm{ee}} \end{pmatrix}, \tag{18}$$

i.e. with $j = \mathrm{i}, \mathrm{e}$ and $l = \mathrm{i}, \mathrm{e}$ we have:

$$\underline{\underline{K}}_{jl} = \int\int\int_V \underline{\underline{B}}_j^{\mathrm{T}}\,\underline{\underline{C}}\,\underline{\underline{B}}_l \,\mathrm{d}V. \tag{19}$$

We may transform the integration over the element volume V into an integration over the volume of the representative master element:

$$\underline{\underline{K}}_{jl} = \int_{-1}^{+1}\int_{-1}^{+1}\int_{-1}^{+1} \underline{\underline{B}}_j^{\mathrm{T}}\,\underline{\underline{C}}\,\underline{\underline{B}}_l \det(\underline{\underline{J}})\,\mathrm{d}\xi\,\mathrm{d}\eta\,\mathrm{d}\zeta. \tag{20}$$

In this representation for $\underline{\underline{K}}_{jl}$, the integration with respect to the radial coordinate ξ can be performed in a closed-form analytical way since the resultant expression is a polynomial in ξ. Inserting the operator matrices $\underline{\underline{B}}_j$ and $\underline{\underline{B}}_l$ and the Jacobian determinant $\det(\underline{\underline{J}})$ yields the stiffness matrices $\underline{\underline{K}}_{jl}$ decomposed into powers of the infinitesimal cell width w:

$$\underline{\underline{K}}_{jl} = \frac{1}{w}\underline{\underline{K}}^0_{jl} + \underline{\underline{K}}^1_{jl} + w\underline{\underline{K}}^2_{jl} \tag{21}$$

with the submatrices $\underline{\underline{K}}^0_{jl}$, $\underline{\underline{K}}^1_{jl}$ and $\underline{\underline{K}}^2_{jl}$ being defined as

$$\begin{aligned}
&\underline{\underline{K}}^0_{jl} = \xi_j\xi_l\underline{\underline{E}}^0, \quad \underline{\underline{K}}^1_{jl} = \xi_j\xi_l\underline{\underline{E}}^0 + \frac{\xi_l}{2}\underline{\underline{E}}^1 + \frac{\xi_j}{2}\underline{\underline{E}}^{1^{\mathrm{T}}},\\
&\underline{\underline{K}}^2_{jl} = \frac{\xi_j\xi_l}{3}\underline{\underline{E}}^0 + \left(\frac{\xi_l}{4} + \frac{\xi_j\xi_l}{12}\right)\underline{\underline{E}}^1 + \left(\frac{\xi_j}{4} + \frac{\xi_j\xi_l}{12}\right)\underline{\underline{E}}^{1^{\mathrm{T}}} + \left(\frac{1}{4} + \frac{\xi_j\xi_l}{12}\right)\underline{\underline{E}}^2.
\end{aligned} \tag{22}$$

The newly introduced matrices $\underline{\underline{E}}^0$, $\underline{\underline{E}}^1$ and $\underline{\underline{E}}^2$ are functions of the circumferential coordinates η, ζ only and usually require numerical evaluation. They are independent from the radial coordinate:

$$\begin{aligned}
&\underline{\underline{E}}^0 = \int_{-1}^{+1}\int_{-1}^{+1} \underline{\underline{B}}^{1^{\mathrm{T}}}\underline{\underline{C}}\underline{\underline{B}}^1 \det(\underline{\bar{J}})\,\mathrm{d}\eta\,\mathrm{d}\zeta, \quad \underline{\underline{E}}^1 = \int_{-1}^{+1}\int_{-1}^{+1} \underline{\underline{B}}^{2^{\mathrm{T}}}\underline{\underline{C}}\underline{\underline{B}}^1 \det(\underline{\bar{J}})\,\mathrm{d}\eta\,\mathrm{d}\zeta,\\
&\underline{\underline{E}}^2 = \int_{-1}^{+1}\int_{-1}^{+1} \underline{\underline{B}}^{2^{\mathrm{T}}}\underline{\underline{C}}\underline{\underline{B}}^2 \det(\underline{\bar{J}})\,\mathrm{d}\eta\,\mathrm{d}\zeta.
\end{aligned} \tag{23}$$

Therein, $\underline{\bar{J}}$ is a reduced Jacobian matrix which only depends on the two circumferential coordinates η, ζ. The relationship between the nodal forces and the nodal displacements of the finite-element cell Ω_{ie} can be written in a decomposed notation with portions corresponding to nodes on the interior boundary Γ_{i} and the exterior boundary Γ_{e} as

$$\underline{\underline{K}}\underline{u} = \begin{bmatrix} \underline{\underline{K}}_{\mathrm{ii}} & \underline{\underline{K}}_{\mathrm{ie}} \\ \underline{\underline{K}}_{\mathrm{ei}} & \underline{\underline{K}}_{\mathrm{ee}} \end{bmatrix} \begin{pmatrix} \underline{u}_{\mathrm{i}} \\ \underline{u}_{\mathrm{e}} \end{pmatrix} = \begin{pmatrix} \underline{P}_{\mathrm{i}} \\ \underline{P}_{\mathrm{e}} \end{pmatrix} = \underline{P}. \tag{24}$$

Multiplying the displacements $\underline{u}_j$ of the nodes on the boundary Γ_j with a still unknown boundary stiffness matrix $\underline{\underline{K}}^{\infty}_j$ of the adjacent structure Ω_j leads to the following interaction forces $\underline{R}_j$ acting on the boundary Γ_j:

$$\underline{R}_j = \underline{\underline{K}}^{\infty}_j \underline{u}_j. \tag{25}$$

Note that since we use the same nodal displacements on the boundary Γ_j of the structure Ω_j as well as on the corresponding boundary Γ_j of the finite element cell Ω_{ie}, we automatically enforce compatibility between the finite element cell and the actual unbounded structure. Postulating equilibrium at the boundary Γ_{i} between the structure Ω_{i} and the finite element cell Ω_{ie} and at the boundary Γ_{e} between Ω_{e} and Ω_{ie} yields a relation between the forces $\underline{R}_j$ on the boundary Γ_j and the nodal forces $\underline{P}_j$ of the finite element cell:

$$\underline{P}_{\mathrm{i}} = \underline{R}_{\mathrm{i}}, \quad \underline{P}_{\mathrm{e}} = -\underline{R}_{\mathrm{e}}. \tag{26}$$

Having established these relations, we may eliminate the forces $\underline{R}_j$ and $\underline{P}_j$ and write the decomposed force–displacement relationship (24) as

$$\begin{bmatrix} \underline{\underline{K}}_{\mathrm{ii}} & \underline{\underline{K}}_{\mathrm{ie}} \\ \underline{\underline{K}}_{\mathrm{ei}} & \underline{\underline{K}}_{\mathrm{ee}} \end{bmatrix} \begin{pmatrix} \underline{u}_{\mathrm{i}} \\ \underline{u}_{\mathrm{e}} \end{pmatrix} = \begin{bmatrix} \underline{\underline{K}}^{\infty}_{\mathrm{i}} & 0 \\ 0 & -\underline{\underline{K}}^{\infty}_{\mathrm{e}} \end{bmatrix} \begin{pmatrix} \underline{u}_{\mathrm{i}} \\ \underline{u}_{\mathrm{e}} \end{pmatrix}. \tag{27}$$

Solving the last of Eq. (27) for $\underline{u}_{\mathrm{e}}$ and resubstituting into the first equation of (27), the validity for arbitrary displacements $\underline{u}_{\mathrm{i}}$ after some algebra leads to the following first relation between the two unknown boundary stiffness matrices $\underline{\underline{K}}^{\infty}_{\mathrm{i}}$ and $\underline{\underline{K}}^{\infty}_{\mathrm{e}}$ which is based on assemblage and compatibility:

$$(\underline{\underline{K}}_{\mathrm{ee}} + \underline{\underline{K}}^{\infty}_{\mathrm{e}})\underline{\underline{K}}^{-1}_{\mathrm{ie}}(\underline{\underline{K}}^{\infty}_{\mathrm{i}} - \underline{\underline{K}}_{\mathrm{ii}}) + \underline{\underline{K}}_{\mathrm{ei}} = 0. \tag{28}$$

Note that as we assume validity of similarity, we may write the following second relation between the two unknown boundary stiffness matrices $\underline{\underline{K}}^{\infty}_{\mathrm{i}}$ and $\underline{\underline{K}}^{\infty}_{\mathrm{e}}$:

$$\underline{\underline{K}}^{\infty}_{\mathrm{e}} = (1+w)\underline{\underline{K}}^{\infty}_{\mathrm{i}}. \tag{29}$$

Using the two relations (28) and (29) between the still unknown boundary stiffness matrices $\underline{\underline{K}}^{\infty}_{\mathrm{i}}$ and $\underline{\underline{K}}^{\infty}_{\mathrm{e}}$, we may derive the following relationship:

$$(\underline{\underline{K}}^{\infty}_{\mathrm{e}} + \underline{\underline{E}}^1)\underline{\underline{E}}^{0-1}(\underline{\underline{K}}^{\infty}_{\mathrm{i}} + \underline{\underline{E}}^{1\mathrm{T}}) - \frac{1}{w}(\underline{\underline{K}}^{\infty}_{\mathrm{e}} - \underline{\underline{K}}^{\infty}_{\mathrm{i}}) - \underline{\underline{E}}^2 = 0. \tag{30}$$

Performing the limit $w \to 0$ which is equivalent to the limit $r_e \to r_i$ along with the similarity based relation (29) leads to:

$$(\underline{\underline{K}}^{\infty} + \underline{\underline{E}}^{1})\underline{\underline{E}}^{0-1}(\underline{\underline{K}}^{\infty} + \underline{\underline{E}}^{1\mathrm{T}}) - \underline{\underline{K}}^{\infty} - \underline{\underline{E}}^{2} = \underline{\underline{0}} \tag{31}$$

with $\underline{\underline{K}}^{\infty} = \underline{\underline{K}}_{\mathrm{i}}^{\infty}$. This expression represents the so-called consistent infinitesimal finite-element cell equation for statics (see Wolf and Song, 1996a). The only unknown quantity is the boundary stiffness matrix $\underline{\underline{K}}^{\infty}$. After performing some algebra this relation can be rewritten:

$$\underline{\underline{K}}^{\infty}\underline{\underline{E}}^{0-1}\underline{\underline{K}}^{\infty} + \left(\underline{\underline{E}}^{1}\underline{\underline{E}}^{0-1} - \frac{1}{2}\underline{\underline{I}}\right)\underline{\underline{K}}^{\infty} + \underline{\underline{K}}^{\infty}\left(\underline{\underline{E}}^{0-1}\underline{\underline{E}}^{1\mathrm{T}} - \frac{1}{2}\underline{\underline{I}}\right) - \underline{\underline{E}}^{2} + \underline{\underline{E}}^{1}\underline{\underline{E}}^{0-1}\underline{\underline{E}}^{1\mathrm{T}} = 0. \tag{32}$$

This equation is the algebraic Riccati equation governing the unknown boundary stiffness matrix $\underline{\underline{K}}^{\infty}$. The quantity $\underline{\underline{I}}$ is the unity matrix.

Let us now refer to the calculation of displacements, strains and stresses at an arbitrary point of the structure at some distance from the interior boundary Γ_i. The first equation in (27) reads:

$$\underline{\underline{K}}_{\mathrm{ii}}\underline{u}_{\mathrm{i}} + \underline{\underline{K}}_{\mathrm{ie}}\underline{u}_{\mathrm{e}} = \underline{\underline{K}}_{\mathrm{i}}^{\infty}\underline{u}_{\mathrm{i}}. \tag{33}$$

The displacements on the boundaries Γ_i and Γ_e are linked by the following relation for an infinitesimal cell width:

$$\underline{u}_{\mathrm{e}} = \underline{u}_{\mathrm{i}} + \underline{u}_{,r}(r = r_{\mathrm{i}})\,\mathrm{d}r. \tag{34}$$

Note that $dr = wr_i$ holds. Thus, for (33) we may also write:

$$(\underline{\underline{K}}_{\mathrm{ii}} + \underline{\underline{K}}_{\mathrm{ie}})\underline{u}_{\mathrm{i}} + \underline{\underline{K}}_{\mathrm{ie}}dr\underline{u}_{,r}(r = r_{\mathrm{i}}) = \underline{\underline{K}}_{\mathrm{i}}^{\infty}\underline{u}_{\mathrm{i}}. \tag{35}$$

Inserting the expressions for the submatrices $\underline{\underline{K}}_{\mathrm{ii}}$ and $\underline{\underline{K}}_{\mathrm{ie}}$ (21) and again performing the limit $w \to 0$ yields:

$$r\underline{u}_{,r} = -\underline{\underline{E}}^{0-1}(\underline{\underline{K}}^{\infty} + \underline{\underline{E}}^{1\mathrm{T}})\underline{u}. \tag{36}$$

This is a system of linear homogeneous first order differential equations of Euler type with nonconstant coefficients which governs the displacement components with respect to the radial coordinate. The index i is omitted since we refer to an arbitrary radial coordinate r. The solution for $\underline{\underline{K}}^{\infty}$ can be derived as follows. It can be readily shown (Wolf and Song, 1996a) that we may formulate a corresponding eigenvalue problem to the algebraic matrix Riccati equation (32):

$$\underline{\underline{H}}\,\underline{\underline{\Phi}} = \underline{\underline{\Phi}}\,\underline{\underline{\Lambda}}, \tag{37}$$

wherein:

$$\underline{\underline{H}} = \begin{bmatrix} -\underline{\underline{E}}^{0-1}\underline{\underline{E}}^{1\mathrm{T}} + \frac{1}{2}\underline{\underline{I}} & -\underline{\underline{E}}^{0-1} \\ -\underline{\underline{E}}^{2} + \underline{\underline{E}}^{1}\underline{\underline{E}}^{0-1}\underline{\underline{E}}^{1\mathrm{T}} & \underline{\underline{E}}^{1}\underline{\underline{E}}^{0-1} - \frac{1}{2}\underline{\underline{I}} \end{bmatrix}, \quad \underline{\underline{\Phi}} = \begin{bmatrix} \underline{\underline{\Phi}}_{11} & \underline{\underline{\Phi}}_{12} \\ \underline{\underline{\Phi}}_{21} & \underline{\underline{\Phi}}_{22} \end{bmatrix}, \quad \underline{\underline{\Lambda}} = \begin{bmatrix} \underline{\underline{\lambda}} & \underline{\underline{0}} \\ \underline{\underline{0}} & -\underline{\underline{\lambda}} \end{bmatrix}. \tag{38}$$

We denote $\underline{\underline{\lambda}}$ as a diagonal matrix including the eigenvalues of the problem, $\underline{\underline{\Phi}}$ includes the corresponding eigenvectors, the matrix $\underline{\underline{H}}$ is usually denoted as Hamiltonian matrix. It is agreed that the arrangement within the matrix $\underline{\underline{\Lambda}}$ is such that the real parts of the eigenvalues λ_i are always negative, i.e. $\mathrm{Re}(\lambda_i) < 0$, with λ_i being the ith occurring eigenvalue. The stiffness matrix $\underline{\underline{K}}^{\infty}$ can be shown to result in the following expression:

$$\underline{\underline{K}}^{\infty} = \underline{\underline{\Phi}}_{21}\underline{\underline{\Phi}}_{11}^{-1}. \tag{39}$$

Rewriting the first equation of the eigenvalue problem (37) with (38) gives:

$$-\underline{\underline{E}}^{0-1}(\underline{\underline{K}}^{\infty} + \underline{\underline{E}}^{1\mathrm{T}}) = \underline{\underline{\Phi}}_{11}\underline{\underline{\lambda}}\underline{\underline{\Phi}}_{11}^{-1} - \frac{1}{2}\underline{\underline{I}}. \tag{40}$$

Substituting (40) into the set of differential equations (36) yields:

$$r\underline{u}_{,r} = \left(\underline{\underline{\Phi}}_{11}\underline{\underline{\lambda}}\underline{\underline{\Phi}}_{11}^{-1} - \frac{1}{2}\underline{\underline{I}}\right)\underline{u}. \tag{41}$$

The solution can straightforwardly be given in the following form:

$$\underline{u} = \underline{\underline{\Phi}}_{11}\,\mathrm{diag}\left[r^{\lambda_i-\frac{1}{2}}\right]\underline{c}. \tag{42}$$

The free integration constants contained in the vector $\underline{c}$ can be determined from the boundary conditions at the characteristic radial coordinate r_0, i.e. we demand $\underline{u}(r=r_0)=\underline{u}_0$. The final representation for the displacements can then be shown to read:

$$\underline{u} = \underline{\underline{\Phi}}_{11}\,\mathrm{diag}\left[\left(\frac{r}{r_0}\right)^{\lambda_i-\frac{1}{2}}\right]\underline{\underline{\Phi}}_{11}^{-1}\underline{u}_0. \tag{43}$$

From the achieved displacement expression (43), the strains and stresses within the structure can also be derived in a straightforward manner by well-known standard relations. The strains $\underline{\varepsilon}$ within an arbitrary element can be written as

$$\underline{\varepsilon} = \underline{\underline{B}}\underline{u} = \begin{pmatrix}\underline{\underline{B}}_i & \underline{\underline{B}}_e\end{pmatrix}\begin{pmatrix}\underline{u}_i\\ \underline{u}_e\end{pmatrix} \tag{44}$$

with the operator matrices $\underline{\underline{B}}_i$ and $\underline{\underline{B}}_e$ defined in (12). Using (34), the three-dimensional strains result in:

$$\underline{\varepsilon} = \underline{\underline{B}}^1 r_i \underline{u}_{,r}(r=r_i) + \frac{1}{2\left(1+\frac{w}{2}(1+\xi)\right)}\underline{\underline{B}}^2\left(2\underline{u}_i + (1+\xi)w r_i \underline{u}_{,r}(r=r_i)\right). \tag{45}$$

Performing the limit $w \to 0$ leads to the following strain representation:

$$\underline{\varepsilon} = \underline{\underline{B}}^1 r \underline{u}_{,r} + \underline{\underline{B}}^2 \underline{u}. \tag{46}$$

Stresses can then be derived from Hooke's generalized law (17) with (15) and (16).

In essence, it can be concluded that after performing the limit $w \to 0$ and solving the matrix Riccati equation, the BFEM consists of the introduction of a pattern of surface elements on the boundary Γ_i only, hence reducing the spatial dimension of discretization by one. An analytical solution for the displacements with respect to the radial coordinate can be derived whereas in the circumferential directions the method converges in the FEM sense. The solution incorporates singular stresses in a natural way due to the power law form of (43) with respect to the similarity/singularity center S. Hence, the BFEM can be used efficiently in particular for the investigation of stress singularities for several classes of elasticity problems.

The BFEM involves the solution of an eigenvalue problem which is not the case in the FEM or the BEM. Indeed, this costs some numerical effort. The reader should note, however, that in the case of stress concentration problems involving stress singularities the solution of the occurring eigenvalue problem delivers the orders of the stress singularities with high accuracy straight from their actual definition, hence the BFEM should serve us well for the scope of the present paper, i.e. the computation of the orders and modes of three-dimensional stress singularities at vertices of notches and cracks and in particular at interfaces at free laminate edges and corners. This is all the more gratifying since it is well-known that e.g. in standard displacement based FEM procedures the calculation of the orders of stress singularities is computationally expensive due to the necessary high number of elements in the vicinity of the singularity center or the necessity of special element formulations in order to incorporate singular stress behaviour. Further note that in the course of the BFEM, straight crack faces or interfaces between dissimilar materials passing through the similarity center do not need to be discretized.

The BFEM is also suited for the analysis of bounded structures. The derivation of the corresponding equations differs only slightly from that of the unbounded case. Details can be found in e.g. Wolf and Song (1996a). Furthermore, the BFEM of course also allows for the treatment of two-dimensional problems in which cases the formulations simplify significantly. The BFEM discretizations then consist of line elements.

3. Results for the orders and modes of stress singularities

3.1. Prerequisites

Before we address three-dimensional free-corner and free-edge stress singularities, let us test the BFEM formulation against several known closed-form analytical or well established numerical benchmark solutions in

the framework of three-dimensional linear elasticity. Employing a spherical coordinate system r, φ_1, φ_2 (see for example Fig. 6) let us assume that any of the displacement components in the vicinity of a singular point in three-dimensional space can be described by an infinite series expansion in a variable separable form which then also holds true for the occurring stress components:

$$u_i(r,\varphi_1,\varphi_2,\lambda) = \sum_{m=1}^{m=\infty} K_m r^{\lambda_m} g_{im}(\varphi_1,\varphi_2), \tag{47}$$

$$\sigma_{ij}(r,\varphi_1,\varphi_2,\lambda) = \sum_{m=1}^{m=\infty} K_m r^{\lambda_m - 1} f_{ijm}(\varphi_1,\varphi_2). \tag{48}$$

In the radial direction r a behaviour of the state variables in the form of a power law is assumed to hold whereas the angular variations are described by the functions $g_{im}(\varphi_1,\varphi_2)$ and $f_{ijm}(\varphi_1,\varphi_2)$. We denote the generalized stress intensity factors as K_m, the quantities λ_m are eigenvalues that may be either real or complex. When $\mathrm{Re}(\lambda_m) < 1$, the stresses grow without bound for $r \to 0$. For reasons of finite strain energy as well as of finite displacements, we are only interested in the eigenvalues that fulfill the condition $0 < \mathrm{Re}(\lambda_m) < 1$. The real part $\mathrm{Re}(\lambda_m) - 1$ of the exponent of the stress representation (48) is then interpreted as the order of the stress singularity. In the case of complex eigenvalues the order of the stress singularity is characterized by both the real part $\mathrm{Re}(\lambda_m) - 1$ and the imaginary part $\mathrm{Im}(\lambda_m)$. Due to the power law form of the BFEM solution (43) we may directly interpret the numerical results of the eigenvalue problem as the desired eigenvalues of the fracture problems at hand.

3.2. Two-dimensional benchmark examples

3.2.1. A crack in a two-dimensional infinite isotropic plate (Griffith crack)

The situation of a straight crack with the length $2a$ in a two-dimensional infinite isotropic plate with unit thickness (Fig. 4) is a classical problem within the framework of linear fracture mechanics which allows for a closed-form analytical solution. Employing a polar coordinate system r, φ centered at the crack tip and writing the two-dimensional stress field in the array form $\underline{\sigma} = (\,\sigma_{xx} \quad \sigma_{yy} \quad \sigma_{xy}\,)^{\mathrm{T}}$ while assuming only inplane loads, the asymptotic behaviour of the stress field in this special case is known to be of the following kind:

$$\underline{\sigma}(r,\varphi,\lambda_{\mathrm{I}},\lambda_{\mathrm{II}}) = K_{\mathrm{I}} r^{\lambda_{\mathrm{I}}} \underline{f}^{\mathrm{I}}(\varphi) + K_{\mathrm{II}} r^{\lambda_{\mathrm{II}}} \underline{f}^{\mathrm{II}}(\varphi) \tag{49}$$

The quantities K_{I} and K_{II} are the stress intensity factors for mode I and mode II crack opening displacements and are available for a good number of benchmark cases. The angular variations of the stress field for both modes are described by the functions $f^{\mathrm{I}}_{xx}(\varphi)$, $f^{\mathrm{I}}_{yy}(\varphi)$, $f^{\mathrm{I}}_{xy}(\varphi)$ and $f^{\mathrm{II}}_{xx}(\varphi)$, $f^{\mathrm{II}}_{yy}(\varphi)$, $f^{\mathrm{II}}_{xy}(\varphi)$, respectively, which are assembled in the one-dimensional arrays $\underline{f}^{\mathrm{I}}(\varphi)$ and $\underline{f}^{\mathrm{II}}(\varphi)$. The exponents λ_{I} and λ_{II} which characterize the order of the occurring stress singularities are known to be purely real and result in the classical values $\lambda_{\mathrm{I}} = -0.5$ and $\lambda_{\mathrm{II}} = -0.5$ for both modes.

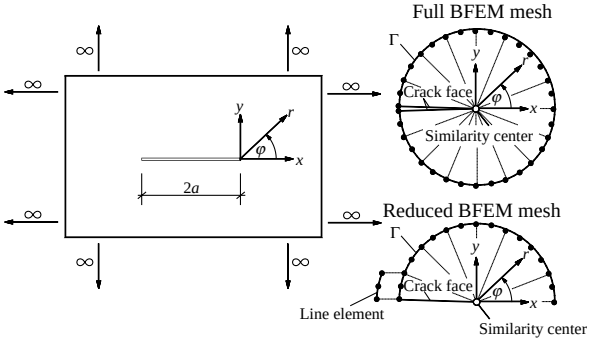

Fig. 4. Griffith crack in an infinite plate, BFEM discretization.

Table 1
Two-dimensional stress singularities at the apex of a Griffith crack

	Symmetric mode (mode I)	Unsymmetric mode (mode II)
Exact solution	−0.500000	−0.500000
BFEM model 1, 6 dof	−0.528763	−0.444275
BFEM model 2, 10 dof	−0.497345	−0.495476
BFEM model 3, 18 dof	−0.499735	−0.499530
BFEM model 4, 34 dof	−0.499981	−0.499966
BFEM model 5, 66 dof	−0.499999	−0.499998
BFEM model 6, 130 dof	−0.500000	−0.500000

The employed BFEM discretization scheme for the vicinity of the Griffith crack is depicted in Fig. 4, right portion, wherein we have taken advantage of the symmetry of the situation: Instead of discretizing the complete boundary, i.e. the unit circle segment Γ enclosed in $-180° \leqslant \varphi \leqslant 180°$ at $r = 1$ (Fig. 4, upper right portion, full BFEM mesh), only the upper half $y \geqslant 0$ of the cracked plate has been considered and the corresponding segment of Γ enclosed in $0 \leqslant \varphi \leqslant 180°$ at $r = 1$ has been discretized by 3-noded line elements (Fig. 4, lower right portion, reduced BFEM mesh). The BFEM node at $x = 1$, $y = 0$ in the symmetry plane is then restricted as follows: For mode I crack opening displacements, we have applied the displacement restriction $u_y = 0$, whereas for mode II crack openings the restriction $u_x = 0$ has been applied at this node. The eigenvalues λ_{I} and λ_{II} according to the BFEM analysis for several discretization stages are compared to the exact values in Table 1. We have computed the eigenvalues λ_{I} and λ_{II} for BFEM model 1 (1 line element, 3 nodes, 6 degrees of freedom (dof)), BFEM model 2 (2 line elements, 5 nodes, 10 dof), BFEM model 3 (4 line elements, 9 nodes, 18 dof), BFEM model 4 (8 line elements, 17 nodes, 34 dof), BFEM model 5 (16 line elements, 33 nodes, 66 dof) and BFEM model 6 (32 line elements, 65 nodes, 130 dof). Note that since we are only interested in the near field behaviour of the stresses, no boundary conditions were imposed on the boundary Γ. This will also be the case for all further two and three-dimensional benchmark examples. The results given in Table 1 reveal that BFEM model 1 with only one single element is too coarse to yield accurate results for the eigenvalues λ_{I} and λ_{II} (the encountered errors result in 5.75% and 11.15% for λ_{I} and λ_{II}, respectively), however by BFEM model 2 with only 2 line elements the error is already well below 1% for both deformation modes which is an overall satisfying yet astonishing result since this means insignificant numerical effort in comparison with full scale FEM computations of comparable accuracy. The results of all further BFEM models show that the convergence behaviour is stable and with BFEM model 6 the exact result is achieved with an accuracy of 6 digits. Note that since we did not apply any boundary conditions on the unit circle segment Γ all computations led to three further eigenvalues which describe the two transitional degrees of freedom of the BFEM mesh in the x and the y-direction, as well as the rotational degree of freedom in the xy-plane.

3.2.2. Straight free interface edge in a laminate consisting of isotropic layers

The situation of free-edge effects in the vicinity of a straight free interface edge between two dissimilar isotropic layer materials (Fig. 5, left portion) can be treated as a quasi two-dimensional problem and a BFEM discretization with 3-noded line elements in the interval $-90° \leqslant \varphi \leqslant 90°$ at $r = 1$ (Fig. 5, right portion) is appropriate. Note that the interface at $y = 0$ is not discretized. The orders of the occurring stress singularities have been determined in a closed-form analytical manner by e.g. Müller et al. (2002) by the method of complex potentials. In this rather general structural situation we may write the asymptotic behaviour of the two-dimensional stress field in the vicinity of the free interface edge as an infinite series as

$$\underline{\sigma}(r, \varphi, \lambda) = \sum_{m=1}^{m=\infty} K_m r^{\lambda_m - 1} \underline{f}_m(\varphi). \tag{50}$$

While the material of layer 2 was assumed as steel with the elastic constants $E_2 = 210\,000$ MPa and $\nu_2 = 0.3$, the modulus of elasticity E_1 of layer 1 was varied wherein the values $E_1 = 160\,000$ MPa, $E_1 = 120\,000$ MPa, $E_1 = 75\,000$ MPa, $E_1 = 50\,000$ MPa and $E_1 = 2100$ MPa were considered. The Poisson's ratio ν_1 was kept invariable as $\nu_1 = 0.3$.

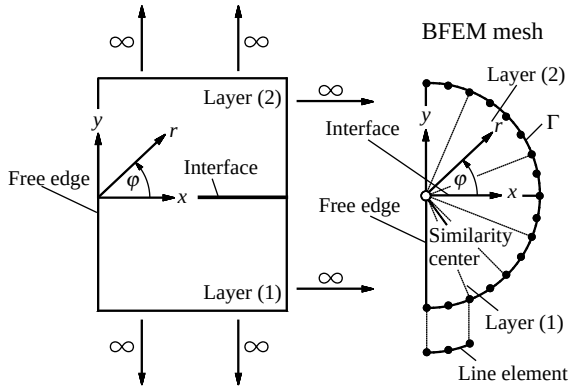

Fig. 5. Free Interface edge in an infinite layered structure with isotropic layer materials, BFEM discretization.

Table 2
Two-dimensional stress singularities at the free interface edge of a laminate consisting of two dissimilar isotropic layers with $\nu_1 = \nu_2 = 0.3$, $E_2 = 210000$ MPa and a varying E_1

Modulus of elasticity E_1 [MPa]	160000	120000	75000	50000	2100
Müller et al. (2002)	−0.006295	−0.025089	−0.072197	−0.117507	−0.278034
BFEM model 1, 10 dof	−0.006460	−0.025854	−0.074972	−0.122581	−0.290476
BFEM model 2, 18 dof	−0.006258	−0.024975	−0.072057	−0.117493	−0.278852
BFEM model 3, 34 dof	−0.006293	−0.025081	−0.072186	−0.117504	−0.278087
BFEM model 4, 66 dof	−0.006295	−0.025089	−0.072196	−0.117506	−0.278037
BFEM model 5, 130 dof	−0.006295	−0.025089	−0.072197	−0.117507	−0.278034

We have employed five different BFEM models for this case which are BFEM model 1 (2 line elements, 5 nodes, 10 dof), BFEM model 2 (4 line elements, 9 nodes, 18 dof), BFEM model 3 (8 line elements, 17 nodes, 34 dof), BFEM model 4 (16 line elements, 33 nodes, 66 dof) and BFEM model 5 (32 line elements, 65 nodes, 130 dof). The eigenvalues as found by the BFEM for several discretization schemes are compared to the exact values of Müller et al. (2002) in Table 2. In all considered cases there occurred only one relevant eigenvalue which was furthermore always found to be purely real. Note that the results as generated by BFEM model 1 are already within an astonishing degree of accuracy in all cases. Again, the BFEM shows a stable convergence behaviour towards the exact analytical solution and with BFEM model 5 the exact result is found again with an accuracy of 6 digits.

3.3. Three-dimensional benchmark examples

3.3.1. 3D stress singularities at the apex of a circular cone

The situation of a conical cone consisting of isotropic material with Young's modulus E and Poisson's ratio ν has been adressed analytically by Bazant and Keer (1974). The cone fills the space r, $0 \leqslant \varphi_1 \leqslant \gamma$, $0 \leqslant \varphi_2 \leqslant 360°$ (Fig. 6) and is considered under two different sets of boundary conditions on the cone boundary Γ_C, namely (i) homogeneous stress boundary conditions on Γ_C and (ii) homogeneous displacement boundary conditions on Γ_C. The first set of boundary conditions corresponds to a free cone whereas the second set describes a rigidly clamped cone and is thus to be regarded as a composite structure with a severe mismatch of material properties. At the cone apex $x = y = z = 0$ a stress singularity is expected to occur. In the present case no local BFEM mesh refinement is necessary since no singular points are to be discretized. Hence, the applied boundary discretization of the unit sphere segment Γ at $r = 1$ with 8-noded surface elements with the similarity center placed at the singular point has been chosen such that a regular meshing scheme with quadrangular element shapes results. For the case of a free cone with $\gamma = 120°$ we have computed the orders $\mathrm{Re}(\lambda_m) - 1$ of the stress singularities for the Poisson's ratios $\nu = 0.0$, $\nu = 0.1$, $\nu = 0.2$ and $\nu = 0.3$ with three different BFEM meshes (see Fig. 7), namely with BFEM model 1 (12 surface elements, 45 nodes, 135 dof), BFEM model 2 (48 surface elements, 161 nodes, 483

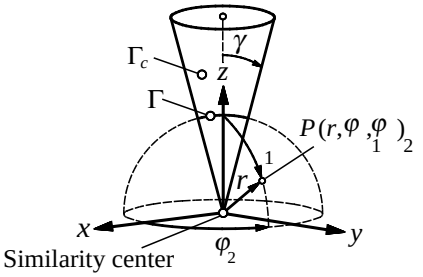

Fig. 6. Conical cone.

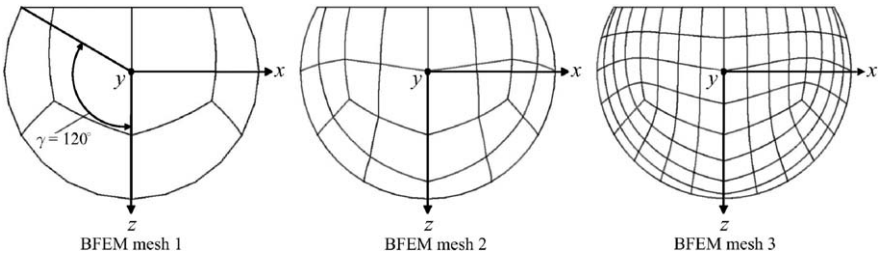

Fig. 7. BFEM meshes for a conical cone with $\gamma = 120°$.

dof) and BFEM model 3 (192 surface elements, 609 nodes, 1827 dof). The results for $\mathrm{Re}(\lambda_m) - 1$ which were all found to be purely real are given in Table 3. It is observed that even with the lowest mesh density the BFEM results match with the solution of Bazant and Keer (1974) up to at least two significant digits. For all further computations we have used model 2 or similar meshes.

As in Bazant and Keer (1974) we have investigated several cone angles γ with $\gamma = 91.8°$, $\gamma = 105°$, $\gamma = 120°$, $\gamma = 135°$, $\gamma = 150°$ and $\gamma = 165°$ and computed the orders $\mathrm{Re}(\lambda_m) - 1$ of the occurring stress singularities for several Poisson's ratios of the cone material. Results for $\mathrm{Re}(\lambda_m) - 1$ for the free cone as well as for the rigid inclusion are given in Fig. 8. For all geometry, material data and boundary conditions considered, the

Table 3
Three-dimensional stress singularities at the apex of a free conical cone in an isotropic halfspace with $\gamma = 120°$ and $v = 0.0$, $v = 0.1$, $v = 0.2$ and $v = 0.3$

Poisson's ratio v	0.0	0.1	0.2	0.3
Bazant and Keer (1974)	−0.1666	−0.1928	−0.2219	−0.2544
BFEM model 1, 135 dof	−0.1661	−0.1921	−0.2208	−0.2524
BFEM model 2, 483 dof	−0.1665	−0.1927	−0.2218	−0.2541
BFEM model 3, 1827 dof	−0.1666	−0.1928	−0.2219	−0.2543

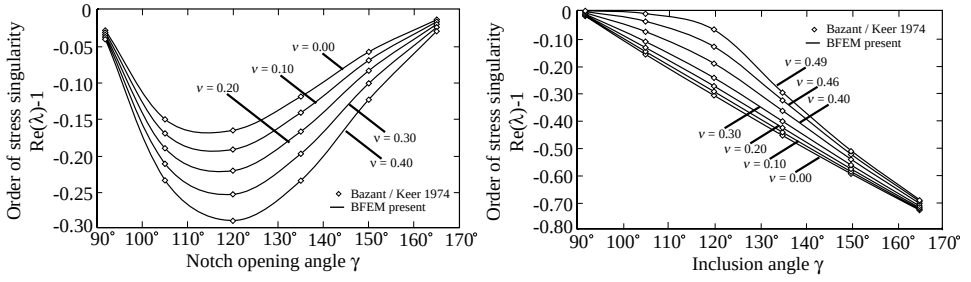

Fig. 8. Three-dimensional stress singularities at the apex of an isotropic cone (left portion) and of a rigid inclusion in an isotropic space (right portion) with varying opening angle γ and Poisson's ratio v.

comparison between the BFEM computations and the results of Bazant and Keer (1974) reveals excellent agreement and in all cases leads to purely real eigenvalues. Further eigenvalues that were detected by the BFEM but were not reported by Bazant and Keer (1974) will not be discussed here for brevity. Since no boundary conditions were formulated concerning the unit circle segment Γ, all computations led to six further eigenvalues, three of which describing the three-dimensional transitional degrees of freedom of the BFEM mesh in all three coordinate directions, as well as three eigenvalues corresponding to the three-dimensional rotational degrees of freedom with respect to all three coordinate axes. Note that these six additional eigenvalues also occurred in the course of all other subsequent three-dimensional BFEM computations as well.

3.3.2. 3D stress singularities at the vertex of a surface breaking crack in an isotropic halfspace

The problem of a surface breaking crack in an isotropic halfspace with the crack front perpendicular to the free surface (Fig. 9), where at the crack vertex $x = y = z = 0$ a stress singularity occurs, has been addressed by a good number of authors. Benthem (1977) computed the orders and modes of the occurring crack stress singularities for different Poisson's ratios by solving a three-dimensional determinantial equation that resulted from the application of Boussinesq–Papkovich–Neuber stress functions in the form of a harmonic representation after utilizing a technique using a separational form of the solution. The finite difference method was utilized by Benthem (1980). Among others, Bazant and Estenssoro (1979), Yamada and Okumara (1981), Somaratna and Ting (1986) and Picu and Gupta (1997) presented numerical results by employing a FEM eigenanalysis technique. Barsoum (1990) used the so-called finite element iterative method. The cracked solid is located in the interval r, $0 \leqslant \varphi_1 \leqslant 90°$, $0 \leqslant \varphi_2 \leqslant 360°$, the stress free crack surfaces are found in the ranges r, $0 \leqslant \varphi_1 \leqslant 90°$, $\varphi_2 = 0$ and r, $0 \leqslant \varphi_1 \leqslant 90°$, $\varphi_2 = 360°$. With the presently chosen coordinates, the crack front coincides with the positive z-axis, the area at $z = 0$ is the stress free surface of the halfspace.

In order to gain an insight into the required discretization strategy, in a first computation we have used a regular BFEM mesh with 8-noded quadrangular surface elements on the unit sphere Γ at $r = 1$ and have used the symmetry conditions of the given situation: for symmetric deformation modes we have prescribed $u_y = 0$ on the symmetry line Γ_S, whereas for unsymmetric deformation modes we have set $u_x = u_z = 0$ on Γ_S. Hence, only one half of the crack situation had to be discretized, e.g. the half enclosed in r, $0 \leqslant \varphi_1 \leqslant 90°$, $0 \leqslant \varphi_2 \leqslant 180°$. As a first step the Poisson's ratio of the isotropic material of the halfspace was set to $\nu = 0$. The dominating orders of the stress singularities $\mathrm{Re}(\lambda_m) - 1$ in both the symmetric and the unsymmetric deformation case are known to be purely real with exactly $\mathrm{Re}(\lambda_m) - 1 = -0.5$ (see also e.g. Bazant and Estenssoro, 1979). We have used five different regular BFEM meshes wherein the similarity center of the BFEM discretization coincided with the origin of the coordinate system (see Fig. 10), namely BFEM model 1 (6 surface elements, 27 nodes, 81 dof), BFEM model 2 (24 surface elements, 89 nodes, 267 dof), BFEM model 3 (54 surface elements, 187 nodes, 561 dof), BFEM model 4 (96 surface elements, 321 nodes, 963 dof) and BFEM model 5 (150 surface elements, 491 nodes, 1473 dof). Table 4 shows the BFEM results for $\mathrm{Re}(\lambda_m) - 1$ as computed by the five different BFEM models. Secondly, we have discretized the unit sphere Γ at $r = 1$ employing a mesh refinement around the point $x = 0$, $y = 0$, $z = 1$ where the crack front meets the discretized surface Γ and used four different BFEM models, namely BFEM model 1 (14 surface elements, 55 nodes, 165 dof), BFEM model 2 (56 surface elements, 193 nodes, 579 dof), BFEM model 3 (126 surface elements, 415 nodes, 1245 dof) and BFEM model 4 (224 surface elements, 721 nodes, 2163 dof). The results for $\mathrm{Re}(\lambda_m) - 1$ are given

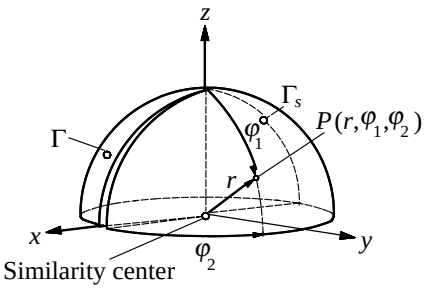

Fig. 9. Surface breaking crack in a halfspace.

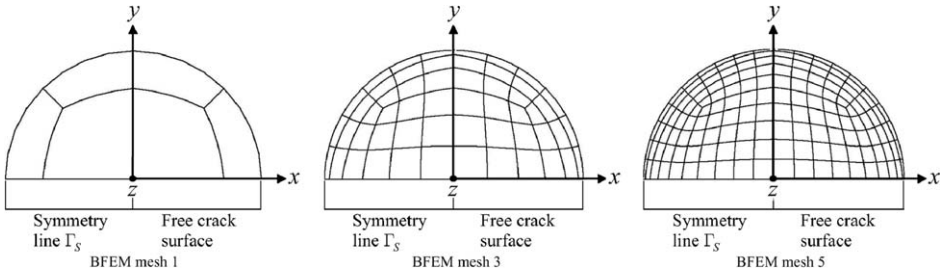

Fig. 10. BFEM meshes for a surface breaking crack in a halfspace, regular meshes.

Table 4
Three-dimensional stress singularities at the vertex of a surface breaking crack in an isotropic halfspace with $\nu = 0.0$, application of regular BFEM meshes

	Symmetric mode	Unsymmetric mode
Bazant and Estenssoro (1979)	−0.5000	−0.5000
BFEM model 1, 81 dof	−0.4765	−0.4620
BFEM model 2, 267 dof	−0.4910	−0.4839
BFEM model 3, 561 dof	−0.4940	−0.4896
BFEM model 4, 963 dof	−0.4955	−0.4923
BFEM model 5, 1473 dof	−0.4964	−0.4938

Table 5
Three-dimensional stress singularities at the vertex of a surface breaking crack in an isotropic halfspace with $\nu = 0.0$, application of refined BFEM meshes

	Symmetric mode	Unsymmetric mode
Bazant and Estenssoro (1979)	−0.5000	−0.5000
BFEM model 1, 165 dof	−0.5017	−0.5009
BFEM model 2, 579 dof	−0.5000	−0.4994
BFEM model 3, 1245 dof	−0.5000	−0.4995
BFEM model 4, 2163 dof	−0.5000	−0.4998

in Table 5, the employed refined BFEM meshes are shown in Fig. 11. In all, it can be stated that the BFEM converges towards the exact solution in both cases of applied meshing schemes. It becomes obvious, however, that simple local mesh refinements at points where the BFEM discretization intersects with the crack front (which is indeed a singular line) ensure a much faster convergence of the results and a better accuracy with significantly less computational effort: the procentual error in the achieved results for $\mathrm{Re}(\lambda_m) - 1$ for both deformation cases is lesser for the coarsest BFEM mesh with local refinements (with 165 dof) than for the finest regular mesh (with 1473 dof) which proves the efficiency of such local mesh refinements. It should be noted, however, that concering the necessity of mesh refinements around singular structural points which intersect with surface discretizations, conflictive opinions can be found in the literature: While e.g. Bazant and Estenssoro (1979) and Somaratna and Ting (1986) claim that uniform meshing schemes are as efficient as locally refined meshes, the overwhelming majority of authors involved with FEM eigenanalyses has employed local mesh refinements with good success which is also in accord with our observations.

Beside the presented convergence characteristics, the results of Table 5 show that the present BFEM computations are in excellent agreement with the exact solution which lends credibility to the BFEM even in three-dimensional cases where singular lines intersect with the surface discretization on Γ. For all further computations we have used the refined BFEM model 4 with which we were able to reproduce the results of e.g. Somaratna and Ting (1986) for varying Poisson's ratios ν with high accuracy (see Fig. 12). For brevity we do not present any results for the occurring lower orders of stress singularities. Furthermore,

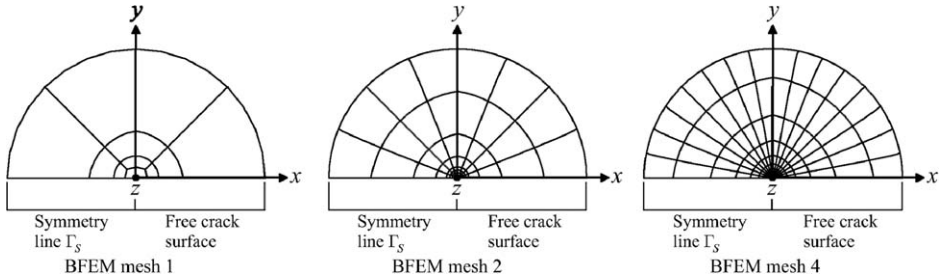

Fig. 11. BFEM meshes for a surface breaking crack in a halfspace, meshes with local refinements.

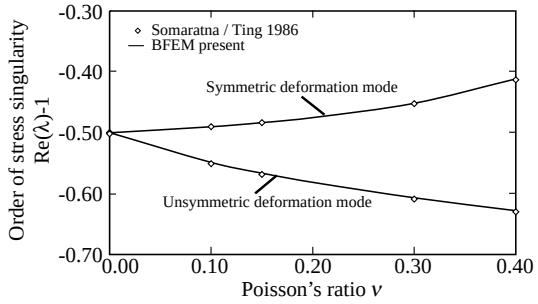

Fig. 12. Three-dimensional stress singularities at the vertex of a surface breaking crack in an isotropic halfspace with varying Poisson's ratio ν.

Table 6
Three-dimensional stress singularities at the vertex of a surface breaking crack in an isotropic halfspace with varying Poisson's ratio ν, comparison of the BFEM results with reference results for symmetric deformation modes

Poisson's ratio ν	0.00	0.10	0.15	0.30	0.40	0.45	0.48
BFEM present	−0.5000	−0.4902	−0.4834	−0.4516	−0.4115	−0.3780	−0.3461
Benthem (1977)	−0.5000	–	−0.4836	−0.4523	−0.4132	–	–
Bazant and Estenssoro (1979)	−0.5000	–	−0.4836	−0.4523	−0.4132	−0.3821	−0.3525
Yamada and Okumara (1981)	−0.4985	–	–	−0.4501	−0.4107	–	–
Somaratna and Ting (1986)	−0.4997	−0.4901	−0.4834	−0.4522	−0.4131	–	–
Barsoum (1990)	−0.5020	–	−0.4867	−0.4557	−0.4162	–	−0.3568
Picu and Gupta (1997)	−0.499	−0.490	–	−0.452	−0.412	–	–

Table 7
Three-dimensional stress singularities at the vertex of a surface breaking crack in an isotropic halfspace with varying Poisson's ratio ν, comparison of the BFEM results with reference results for unsymmetric deformation modes

Poisson's ratio ν	0.00	0.10	0.15	0.30	0.40
BFEM present	−0.4998	−0.5488	−0.5664	−0.6069	−0.6281
Bazant and Estenssoro (1979)	−0.500	−0.548	−0.565	−0.598	−0.604
Benthem (1980)	−0.5000	–	−0.5668	−0.6073	−0.6286
Somaratna and Ting (1986)	−0.5017	−0.5508	−0.5685	−0.6089	−0.6299
Picu and Gupta (1997)	−0.502	−0.551	–	−0.609	−0.630

Tables 6 and 7 show a comparison of the present BFEM results with some of the available results of other authors for several discrete values of the Poisson's ratio ν of the halfspace material. In all cases, a good conformity between the present BFEM and the reference results up to at least two significant digits is found.

The choice of 8-noded elements seems to be an advantageous decision compared to the application of elements with lower order shape functions. As an example, we may cite the pioneering and essential work of Bazant and Estenssoro (1979) who investigated the asymptotic behaviour of the solutions for three-dimensional crack problems by employing a FEM eigenanalysis technique with a finite element surface discretization. Bazant and Estenssoro (1979) were confronted with slow convergence characteristics when applying 4-noded surface elements so that they had to resort to an extrapolation technique in order to achieve sufficiently accurate results. Hence, a good number of other authors who also used an identical eigenfunction expansion approach inspired by Bazant and Estenssoro (1979) frequently applied finite elements with higher order shape functions, among them, e.g. Somaratna and Ting (1986) or Picu and Gupta (1997) who applied a surface discretization with 8-noded elements, or Labossiere and Dunn (2001) and Dimitrov et al. (2001, 2002) who employed 6-noded triangular elements.

3.3.3. 3D stress singularities at the vertex of a surface breaking interface crack between an isotropic halfspace and a rigid substrate

Consider the situation of a straight surface breaking interface crack between an isotropic halfspace and a rigid substrate with the crack front perpendicular to the free surface of the structure. Beside the structural discontinuity introduced by the crack this situation will yield severe stress singularities since this problem describes a composite structure with a serious mismatch in the elastic material parameters. Assuming that the rigid material is found in the interval r, $0 \leqslant \varphi_1 \leqslant 90°$, $180° \leqslant \varphi_2 \leqslant 360°$, we may simulate the interface crack situation by restricting the displacements on Γ_S (Fig. 9) as $u_x = u_y = u_z = 0$ and by discretizing only the half of the unit sphere section Γ at $r = 1$ enclosed in $0 \leqslant \varphi_1 \leqslant 90°$, $0 \leqslant \varphi_2 \leqslant 180°$. The BFEM results for a varying Poisson's ratio ν match those of Barsoum (1990) generated by the FEM iterative method very closely (Fig. 13). In the approximate range of about $0 \leqslant \nu \leqslant 0.20$ the dominating eigenvalue is complex. For values of approximately $\nu > 0.2$ this eigenvalue splits into two separate real eigenvalues. Hence, we have an additional logarithmic stress singularity at the bifurcation point. An additional real eigenvalue of lower power appears in the range of approximately $0 \leqslant \nu \leqslant 0.24$.

3.4. Three-dimensional stress singularities in laminate elasticity: free-edge and free-corner effects

3.4.1. Prerequisites

In the present contribution the main emphasis is put on the computation of the orders of stress singularities, characterized by $\mathrm{Re}(\lambda_m) - 1$ and $\mathrm{Im}(\lambda_m)$, and the corresponding eigenmodes in the vicinity of the interface between two dissimilar laminate layers near free edges and corners (see Fig. 14) of laminated plates. Generally speaking, those real parts $\mathrm{Re}(\lambda_m) - 1$ of the problem eigenvalues which induce stress singularities and which possess high absolute values $|\mathrm{Re}(\lambda_m) - 1|$ are often rated as indicators for a "critical" structural situation whereas stress singularities with lower values of $|\mathrm{Re}(\lambda_m) - 1|$ are often understood as being aligned with a lesser "criticality". However, even though correspondent statements can be found in a good number of scientific works, the assessment of the potential criticality of a structural situation with involved stress singularities in terms of the eigenvalues λ_m is somewhat nebulous since an actual conclusive estimation requires the

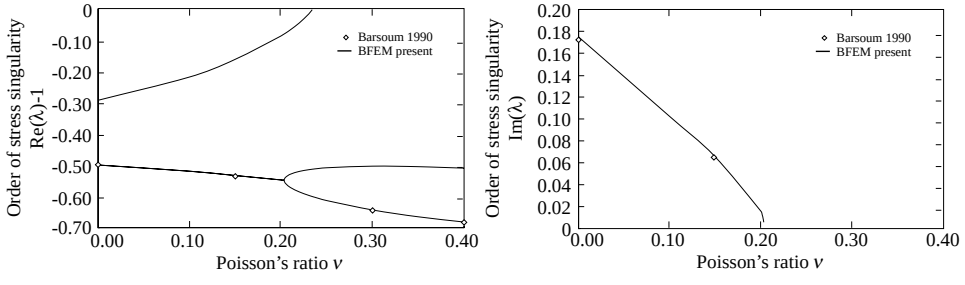

Fig. 13. Three-dimensional stress singularities at the vertex of a surface breaking interface crack between an isotropic halfspace with varying Poisson's ratio ν and a rigid substrate.

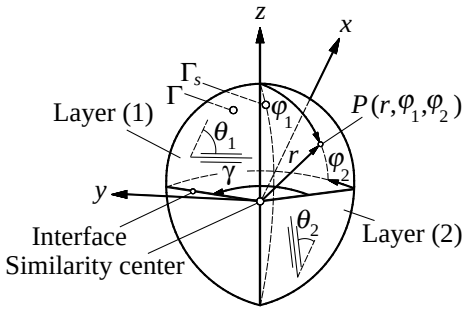

Fig. 14. Free laminate interface corner with arbitrary opening angle γ.

employment of adequate fracture criteria, for example by taking into account the corresponding generalized stress intensity factors. This, however, is well beyond the scope of the present work and must be deferred to future investigations, nevertheless the in-depth study of the problem eigenvalues which describe the orders of the occurring stress singularities is of fundamental interest since these reveal basic characteristics of the asymptotic behaviour of the near field state variables at free edges and corners of composite laminates and enable a first rudimentary assessment of the structural criticality as described above.

Let us investigate the asymptotic behaviour of the state variables in the vicinity of arbitrary bimaterial interface corners with the opening angle γ at the corner tip $x = y = z = 0$ (Fig. 14). From this general corner geometry the special case of a straight free interface edge (i.e. the geometry in which the stress fields are commonly referred to as free-edge effects) can be generated by setting the corner angle to $\gamma = 180°$. The vicinity of the laminate corner is described by the coordinate ranges r, $0 \leqslant \varphi_1 \leqslant 180°$, $0 \leqslant \varphi_2 \leqslant \gamma$ wherein the intervals r, $0 \leqslant \varphi_1 \leqslant 180°$, $\varphi_2 = 0$ and r, $0 \leqslant \varphi_1 \leqslant 180°$, $\varphi_2 = \gamma$ describe the traction free laminate edges which form the corner geometry. The corner interface involves two layers, namely layer 1 enclosed in the region r, $0 \leqslant \varphi_1 \leqslant 90°$, $0 \leqslant \varphi_2 \leqslant \gamma$ and layer 2 which is found in the interval r, $90° \leqslant \varphi_1 \leqslant 180°$, $0 \leqslant \varphi_2 \leqslant \gamma$. If the layer materials are taken to be orthotropic, the orientation angles θ_1 and θ_2 measured from the x-axis describe the layerwise principal material directions in the xy-plane so that as the most general laminate case we consider a $[\theta_1/\theta_2]$-interface. The interface between the two adjacent layers coincides with the xy-plane at $z = 0$. Analogously to the preceding benchmark examples, the surface Γ of the unit sphere section at $r = 1$ has been discretized with 8-noded quadrangular surface elements. Note that the similarity center of the BFEM discretization again coincides with the singular corner tip point at $x = y = z = 0$ so that the BFEM displacement solution (43) yields the desired orders of the stress singularities characterized by $\mathrm{Re}(\lambda_m) - 1$ and $\mathrm{Im}(\lambda_m)$ in a straightforward way. Again, since we are only interested in the eigenvalues and eigenmodes of the displacements and stresses in the near field of the interface corner point, no boundary conditions are imposed on Γ.

3.4.2. 3D stress singularities at rectangular interface corners of laminates with isotropic layers

Let us consider straight free edges ($\gamma = 180°$) and rectangular corners ($\gamma = 90°$) of laminates consisting of purely isotropic layers. The linear elastic material behaviour of layer 1 is assumed to be described by the modulus of elasticity E_1 and the Poisson's ratio ν_1 while layer 2 has the elastic properties E_2 and ν_2. For both the edge and the corner geometry, advantage can be taken of the symmetry properties of the given situation by only considering the half enclosed in the interval r, $0 \leqslant \varphi_1 \leqslant 180°$, $0 \leqslant \varphi_2 \leqslant \frac{\gamma}{2}$. For symmetric deformation modes, zero displacements $u_y = 0$ can then be prescribed on the symmetry line Γ_S at $r = 1$, $0 \leqslant \varphi_1 \leqslant 180°$, $\varphi_2 = \frac{\gamma}{2}$, whereas for unsymmetric deformation modes the constraints $u_x = u_z = 0$ on Γ_S hold. Since the open literature does not contain any information on the convergence properties of FEM techniques employing surface discretizations in the present situation of interface corners, for comparison purposes we have considered rectangular corners with $\gamma = 90°$ and again employed surface meshes on the unit sphere section Γ with regular element schemes. Furthermore we have calculated the orders of the stress singularities generated by BFEM meshes with local refinements in the vicinity of the two points $r = 1$, $\varphi_1 = 90°$, $\varphi_2 = 0$ and $r = 1$, $\varphi_1 = 90°$, $\varphi_2 = \gamma$ where the two free-edge interfaces intersect with the BFEM discretization. The locally refined meshes

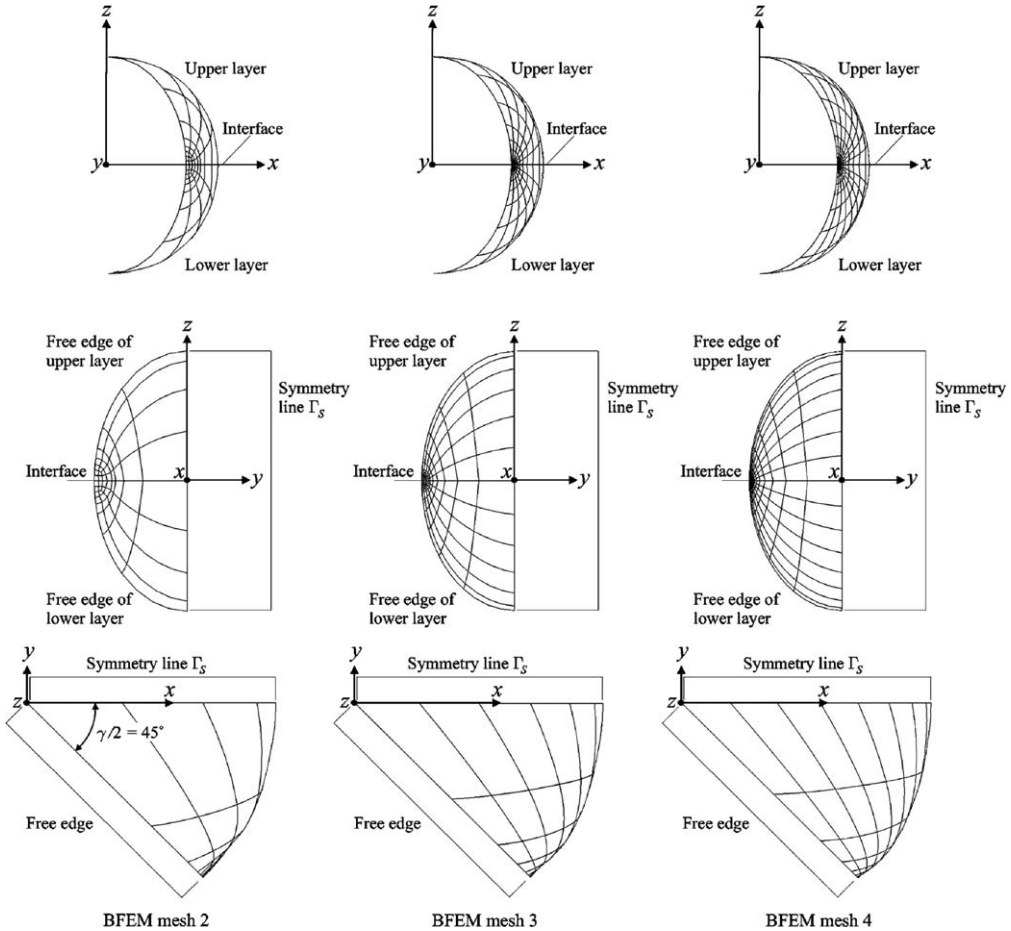

Fig. 15. BFEM meshes for a free rectangular laminate interface corner with isotropic layers, application of locally refined half models, consideration of symmetry properties.

are depicted in Fig. 15. We have employed 6 regular meshes in all, namely BFEM mesh 1 (6 elements, 27 nodes, 81 dof), BFEM mesh 2 (24 elements, 89 nodes, 267 dof), BFEM mesh 3 (54 elements, 187 nodes, 561 dof), BFEM mesh 4 (96 elements, 321 nodes, 963 dof), BFEM mesh 5 (150 elements, 491 nodes, 1473 dof) and BFEM mesh 6 (294 elements, 939 nodes, 2817 dof), and 4 BFEM meshes with local refinements in the vicinity of the interface edge points, namely refined BFEM mesh 1 (14 elements, 55 nodes, 165 dof), refined BFEM mesh 2 (56 elements, 193 nodes, 579 dof), refined BFEM mesh 3 (126 elements, 415 nodes, 1245 dof) and refined BFEM mesh 4 (224 elements, 721 nodes, 2163 dof). Note that in the case of the regular meshes we did not take advantage of the symmetry properties which, however, has been done for the locally refined meshes. The results for aluminium and epoxy corners with the elastic properties $E_1 = 70\,000$ MPa, $\nu_1 = 0.33$, $E_2 = 2980$ MPa, $\nu_2 = 0.38$ are given in Tables 8 and 9 for the regular and the refined BFEM meshes

Table 8
Three-dimensional stress singularities at the tip of a free rectangular corner of a laminate consisting of isotropic layers, layer 1: aluminium, layer 2: epoxy, application of regular BFEM meshes

BFEM model 1, 81 dof	−0.3495
BFEM model 2, 267 dof	−0.3561
BFEM model 3, 561 dof	−0.3572
BFEM model 4, 963 dof	−0.3576
BFEM model 5, 1473 dof	−0.3578
BFEM model 6, 2817 dof	−0.3580

Table 9
Three-dimensional stress singularities at the tip of a free rectangular corner of a laminate consisting of isotropic layers, layer 1: aluminium, layer 2: epoxy, application of refined BFEM meshes

BFEM model 1, 165 dof	−0.3571
BFEM model 2, 579 dof	−0.3584
BFEM model 3, 1245 dof	−0.3584
BFEM model 4, 2163 dof	−0.3584

in the case of symmetric deformation modes. The results again reveal that the utilization of uniform meshing schemes on Γ leads to quite slow convergence rates. On the other hand, however, it is observed that by the application of the refined BFEM meshes convergent results are already achieved with the refined BFEM mesh 2, thus again indicating the efficiency of the BFEM when simple local mesh refinements are applied. Note that for the present corner interface the consideration of unsymmetric deformation modes did not lead to any stress singularities. For all subsequent computations on free-edge and free-corner singularities in layered structures with isotropic layers we have employed the refined BFEM mesh 3 with 1245 degrees of freedom under consideration of the symmetry properties of the corner situation.

For the present situation of a three-dimensional rectangular bimaterial joint it is of basic interest to investigate the influence of the elastic layer properties on the orders $\mathrm{Re}(\lambda_m) - 1$ and $\mathrm{Im}(\lambda_m)$ of the corner stress singularities. In all subsequent computations we have kept E_2 and ν_2 constant as $E_2 = 210\,000$ MPa and $\nu_2 = 0.3$ while we have investigated the asymptotic behaviour of the displacements and stresses at the rectangular free bimaterial interface corner for the discrete values $E_1 = 2100$ MPa, $E_1 = 50\,000$ MPa, $E_1 = 75\,000$ MPa, $E_1 = 120\,000$ MPa, $E_1 = 160\,000$ MPa and $E_1 = 210\,000$ MPa with a varying Poisson's ratio ν_1 in the range $-1 \leqslant \nu_1 < 0.5$. Furthermore, it will be an interesting aspect to compare the three-dimensional corner singularities to those as they occur at the two converging free edges which eventually form the free corner. To begin with, we have computed the orders of the stress singularities for the free-edge situation ($\gamma = 180°$) and, instead of using a three-dimensional BFEM model, we have conveniently employed a two-dimensional BFEM mesh with line elements on a half segment of the unit circle at $r = 1$ (compare also Fig. 5) which is equivalent to the two-dimensional BFEM model 5 with 32 3-noded line elements, 65 nodes and 130 degrees of freedom as employed in Section 3.2.2. The results for the problem eigenvalues are given in Fig. 16. For each material combination with involved stress singularities only one relevant eigenvalue occurrs, and all relevant eigenvalues are found to be purely real and to be confined to an interval for the Poisson's ratio ν_1 of approximately $0 < \nu_1 < 0.5$. It is obvious that with an increasing mismatch in the elastic properties of the adjacent layers (i.e. a decreasing ratio E_1/E_2), the severity of the occurring stress singularities is amplified. As a consequence, maximum absolute values $|\mathrm{Re}(\lambda_m) - 1|$ are found in the case of $E_1 = 2100$ MPa for higher positive values of ν_1, while with increasing values for E_1 the orders $|\mathrm{Re}(\lambda_m) - 1|$ decrease. The value range of ν_1 in which stress singularities occur is also diminished with increasing E_1: as an example, in the case of $E_1 = 160\,000$ MPa stress

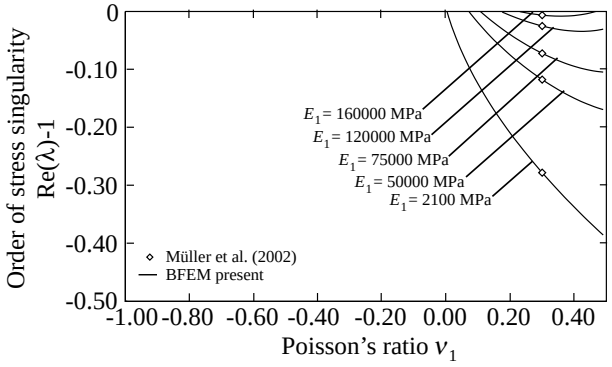

Fig. 16. Two-dimensional stress singularities at the free interface edge of a laminate consisting of isotropic layers with varying modulus of elasticity E_1 and Poisson's ratio ν_1.

singularities are encountered only in the interval of about $0.23 < \nu_1 < 0.47$. Note that the BFEM results match excellently with the analytical results of Müller et al. (2002). Further note that in the case of $E_1 = 210\,000$ MPa no stress singularities at all occur in the free-edge situation which is a remarkable and somewhat unexpected outcome.

The resultant orders of the stress singularities in the situation of a rectangular free interface corner ($\gamma = 90°$) with adjacent isotropic layers for analogous material combinations as in the described free-edge case are depicted in Fig. 17 for the symmetric deformation mode. Results for the unsymmetric deformation mode are given in Fig. 18. Considering the symmetric deformation mode it is revealed that for Poisson's ratios $\nu_1 > 0$, for each considered material combination for which stress singularities arise there always occurs only one relevant purely real eigenvalue (Fig. 17). The overall shapes of the resultant curve plots are very similar to those of the free-edge case (the results of which we have also included in Fig. 17), however it also becomes clear that the free-corner singularities in all exhibit higher absolute real values $|\mathrm{Re}(\lambda_m) - 1|$ for all considered cases of material combinations. The value ranges for ν_1 in which stress singularities arise are larger than those of the free-edge situation. This hints of a generally higher criticality of the free-corner case when compared to the classical situation of the free-edge effect. Note that the minimum eigenvalue $\mathrm{Re}(\lambda_m) - 1 = -0.4483$ is found for $E_1 = 2100$ MPa and $\nu_1 = 0.49$ which describes a corner stress singularity which nearly amounts to the classical Griffith crack value of $\mathrm{Re}(\lambda_m) - 1 = -0.5$. Again, in the case of $E_1 = 210\,000$ MPa no stress singularities occur for positive values of ν_1. Note, however, that unlike in the free-edge case, stress singularities are also encountered when considering negative values for the Poisson's ratio ν_1. The occurring eigenvalues are all found to be complex (i.e. $\mathrm{Im}(\lambda_m)$ is nonvanishing, see Fig. 17) which leads to oscillating eigenmodes in the vicinity of the singular point. The relevant eigenvalues are confined to an interval of about $-1.00 \leqslant \nu_1 < -0.42$ for $E_1 = 2100$ MPa. The value ranges for $\nu_1 < 0$ in which stress singularities arise actually decrease with increasing E_1 which also holds for the encountered absolute values of the real parts $|\mathrm{Re}(\lambda_m) - 1|$ and the resultant imaginary parts $\mathrm{Im}(\lambda_m)$. Again, it is found that higher degrees of mismatches in the linear elastic material

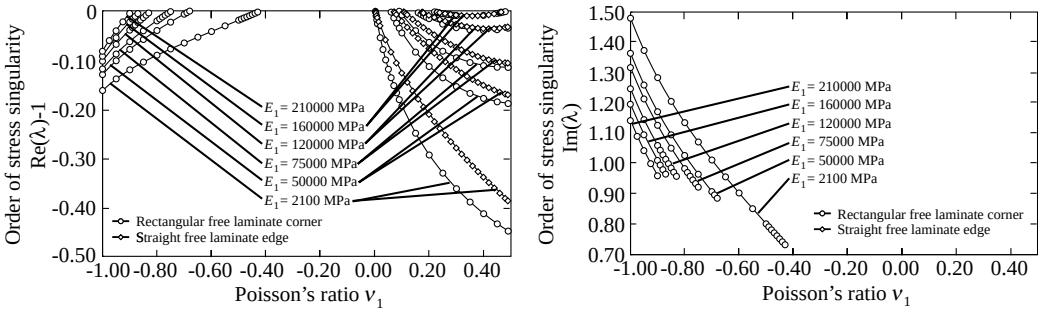

Fig. 17. Three-dimensional stress singularities at the tip of a rectangular interface corner of a laminate with isotropic layers with varying modulus of elasticity E_1 and Poisson's ratio ν_1, symmetric mode.

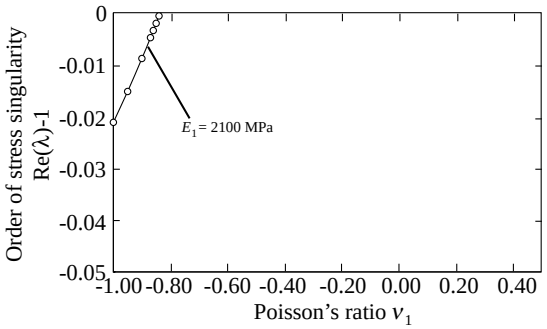

Fig. 18. Three-dimensional stress singularities at the tip of a rectangular interface corner of a laminate with isotropic layers with varying modulus of elasticity E_1 and Poisson's ratio ν_1, unsymmetric mode.

properties of the adjacent layers also lead to more significant stress singularities. Note that for the case of $E_1 = 210\,000$ MPa there also occur some weak stress singularities in the interval of about $-1.00 \leqslant v_1 < -0.90$. In the case of unsymmetric deformation modes, eigenvalues which lead to stress singularities are found only for the case of $E_1 = 2100$ MPa in the range of approximately $-1.00 \leqslant v_1 < -0.84$. The encountered eigenvalues are all found to be real and to be of very low order which reflects a weak stress singularity. For all other considered material combinations no stress singularities occur for unsymmetric deformation modes which again comes as an unexpected result.

3.4.3. 3D stress singularities at rectangular interface corners of laminates with monotropic layers

Beside the previously discussed cases of straight free edges and free rectangular corners at interfaces between isotropic laminate layers, there is a special interest in the nature of the free-edge and free-corner stress singularities when laminate interfaces of arbitrary non-orthotropic layups $[\theta_1/\theta_2]$ are dealt with. Presently we have assumed the following linear elastic orthotropic on-axis material properties for a laminate layer consisting of typical fiber reinforced plastic (with x being the direction of the fiber reinforcements):

$$E_{xx} = 138\,000 \text{ MPa}, \quad E_{yy} = 14\,500 \text{ MPa}, \quad E_{zz} = 14\,500 \text{ MPa},$$
$$G_{xy} = 5860 \text{ MPa}, \quad G_{xz} = 5860 \text{ MPa}, \quad G_{yz} = 5860 \text{ MPa},$$
$$v_{xy} = 0.21, \quad v_{xz} = 0.21, \quad v_{yz} = 0.21$$

The structural BFEM model is analogous to the one as depicted in Fig. 14. Note that in the present case of interface layups $[\theta_1/\theta_2]$ no symmetry line Γ_S exists, hence no reduced BFEM models are applicable. In order to gain some insight into the convergence behaviour of the BFEM in the case of a free laminate corner with involved material orthotropy, we have conducted a brief convergence analysis for the two exemplary layups $[\pm 45°]$ and $[0°/90°]$ for a free corner with the opening angle $\gamma = 90°$ and used three different locally refined BFEM meshes on the unit sphere section Γ at $r = 1$, namely BFEM mesh 1 (28 elements, 101 nodes, 303 dof), BFEM mesh 2 (112 elements, 369 nodes, 1107 dof) and BFEM mesh 3 (252 elements, 805 nodes, 2415 dof). In both layup cases, only one relevant and purely real eigenvalue was found. The occurring real parts $\mathrm{Re}(\lambda_m) - 1$ of the eigenvalues for both layups are given in Table 10. It is found that all applied BFEM meshes seem to deliver quite reasonable results wherein BFEM mesh 2 (see Fig. 19) seems to be an appropriate compromise between the achievable accuracy of the results (which is three digits when compared to BFEM mesh 3) and the computational effort that has to be spent. Hence, in all subsequent computations the eigenvalues which characterize the stress singularities at the interface corner points of the layups $[\theta_1/\theta_2]$ have been calculated by BFEM mesh 2 for the fixed material orientation angles $\theta_1 = 0°$, $\theta_1 = 30°$, $\theta_1 = 60°$ and $\theta_1 = 90°$ of layer 1 with a variable material orientation angle θ_2 in layer 2 with $-90° \leqslant \theta_2 \leqslant 90°$ and a step size of $\Delta\theta_2 \leqslant 5°$. Note that the present full BFEM mesh 2 can be constructed from the halfmodel BFEM mesh 2 as it is was used in Section 3.4.2 by mirroring the halfmodel horizontally. Beside the situation of a free rectangular laminate corner with $\gamma = 90°$ we have also computed the orders of the stress singularities for straight free laminate interface edges ($\gamma = 180°$) with identical layups using an analogous BFEM mesh with the same number of nodes and elements as for the free rectangular corner case (see Fig. 19). For all considered layup cases $[0°/\theta_2]$, $[30°/\theta_2]$, $[60°/\theta_2]$ and $[90°/\theta_2]$ and both opening angles $\gamma = 90°$ and $\gamma = 180°$, only one relevant purely real eigenvalue leading to stress singularities occurred (see Fig. 20). As it was also found by other authors in preceding investigations, it can generally be stated that free-edge singularities are of rather low order when compared to classical problems in the framework of fracture mechanics like e.g. the Griffith crack in an isotropic plate. As was to be expected, the eigenvalue distributions concerning the layups $[0°/\theta_2]$ and $[90°/\theta_2]$ are symmetric with respect to the angle $\theta_2 = 0°$. In the case of the $[0°/\theta_2]$–layups, for all considered angles

Table 10
Three-dimensional stress singularities at the tip of free rectangular corners of laminates consisting of orthotropic layers

	$[\pm 45°]$-Interface	$[0°/90°]$-Interface
BFEM model 1, 303 dof	−0.0651	−0.0472
BFEM model 2, 1107 dof	−0.0642	−0.0461
BFEM model 3, 2415 dof	−0.0640	−0.0460

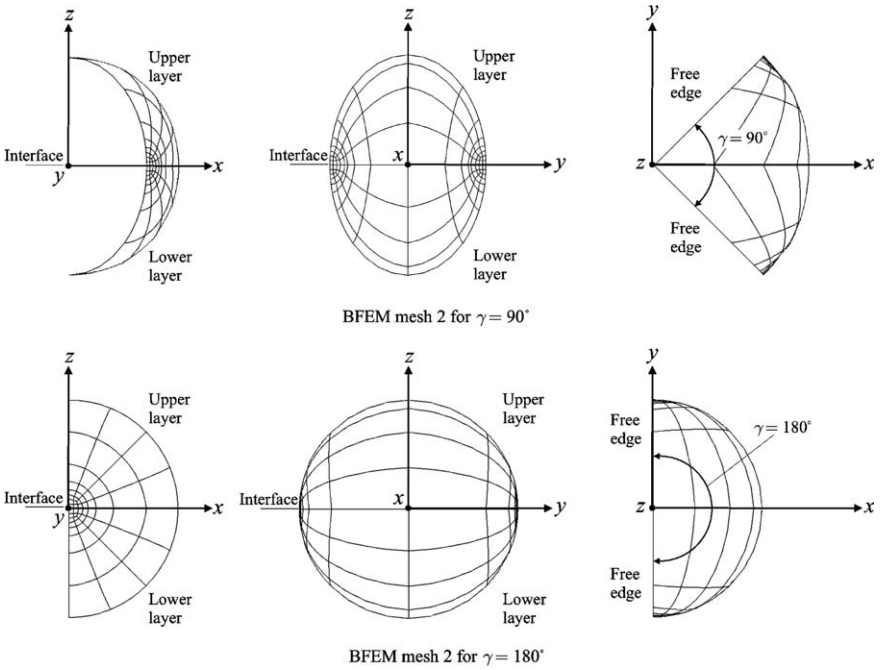

Fig. 19. Locally refined BFEM meshes for a free rectangular interface corner ($\gamma = 90°$) and a straight free interface edge ($\gamma = 180°$) of a laminate consisting of orthotropic layers with arbitrary inplane material orientations.

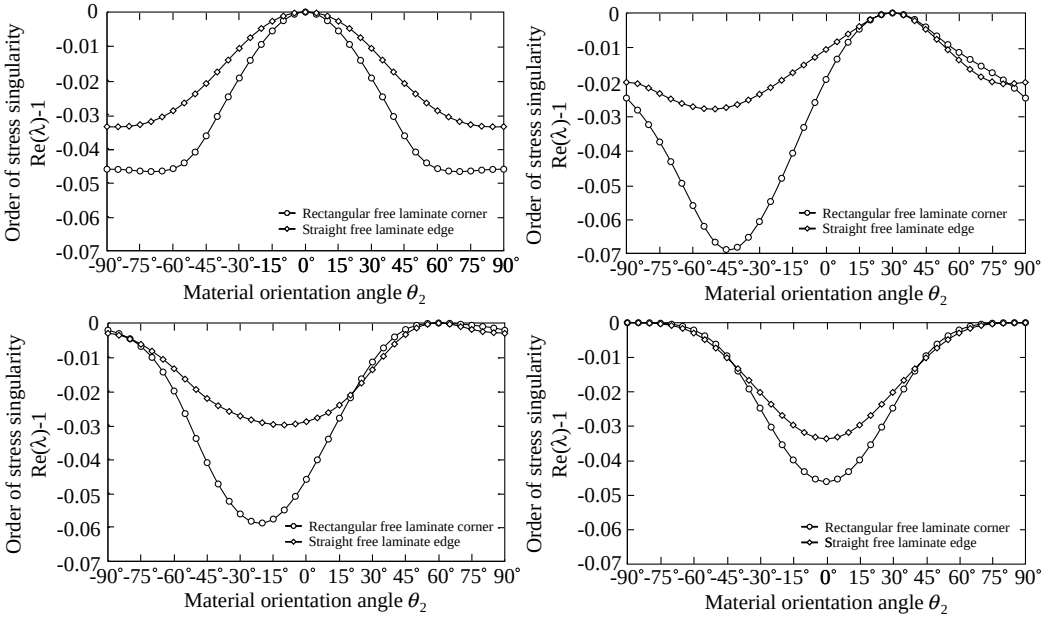

Fig. 20. BFEM results for the orders of stress singularities at rectangular interface corners and straight free laminate interface edges with the layup $[0°/\theta_2]$ (upper left portion), $[30°/\theta_2]$ (upper right portion), $[60°/\theta_2]$ (lower left portion) and $[90°/\theta_2]$ (lower right portion).

θ_2 the absolute values $|\mathrm{Re}(\lambda_m) - 1|$ of the real parts of the eigenvalues which describe the stress singularities in the vicinity of the rectangular corner interface are found to be significantly higher than those of the pure free-edge situation. In the case of the free rectangular corner, the highest absolute value $|\mathrm{Re}(\lambda_m) - 1|$ is found at

$\theta_2 \approx \pm 70°$ which is a somewhat surprising result since by intuition one would probably expect the pure cross-ply interface layup [0°/90°] to yield the most severe stress singularities, which is indeed the case in the free-edge situation where the highest value $|\mathrm{Re}(\lambda_m) - 1|$ is found at $\theta_2 = \pm 90°$. For all further considered layups, with increasing angles θ_1 the values θ_2 for which the maximum absolute values $|\mathrm{Re}(\lambda_m) - 1|$ are determined also increase: for the layups $[30°/\theta_2]$, $[60°/\theta_2]$, and $[90°/\theta_2]$ minimum eigenvalues are encountered for $\theta_2 = -45°$, $\theta_2 = -20°$, and $\theta_2 = 0°$ in the corner free-corner situation, whereas for the pure free-edge case the minimum real parts $\mathrm{Re}(\lambda_m) - 1$ are located at about $\theta_2 = -50°$, $\theta_2 = -10°$, and $\theta_2 = 0°$. For interface layups with $\theta_1 = \theta_2$ we naturally have $\mathrm{Re}(\lambda_m) - 1 = 0$, i.e. no stress singularities occur. Note that even though generally speaking the orders of the free-corner singularities are usually more severe than those in the free-edge situation, for some layup cases in certain value ranges of θ_2, the orders of the occurring free-edge stress singularities are even slightly more critical than those encountered at the free rectangular interface corner with identical layup. This comes as a somewhat surprising result since from intuition it should be expected that the situation of a free rectangular corner always yields the higher criticality: in this situation two straight free edges merge into a free interface corner with the accompanying free-corner stress concentrations. Note, however, that in these cases the absolute values $|\mathrm{Re}(\lambda_m) - 1|$ of the orders of the occurring free-edge singularities are only slightly higher than those of the corresponding free-corner singularities.

As a closure, let us shortly discuss the displacement eigenmodes for the two exemplary layups [0°/90°] (Fig. 21) and [±45°] (Fig. 22) corresponding to those eigenvalues $\mathrm{Re}(\lambda_m) - 1$ which cause corner stress singularities. In the case of the cross-ply interface corner [0°/90°] it is observed that the displacement eigenmode corresponding to the eigenvalue $\mathrm{Re}(\lambda_m) - 1 = -0.0461$ is symmetric with respect to the xz-plane. For the displacements we have $u_x(x,y,z) = u_x(x,-y,z)$, $u_y(x,y,z) = -u_y(x,-y,z)$ and $u_z(x,y,z) = u_z(x,-y,z)$, as was to be

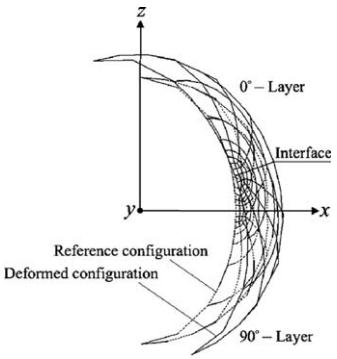

Fig. 21. Displacement eigenmode for a free rectangular interface corner of a laminate with the interface layup [0°/90°] corresponding to the eigenvalue $\mathrm{Re}(\lambda_m) - 1 = -0.0461$.

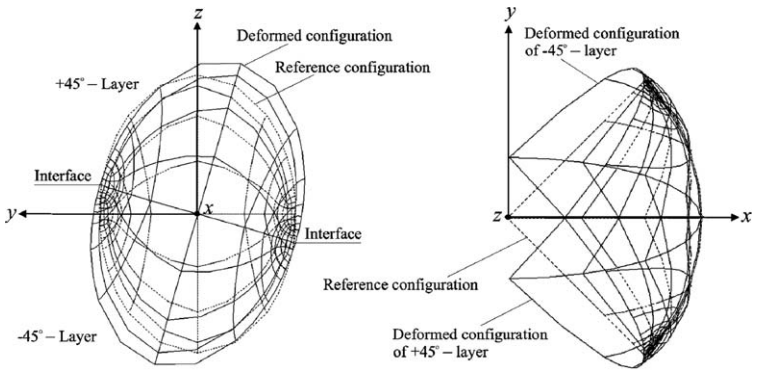

Fig. 22. Displacement eigenmode for a free rectangular interface corner of a laminate with the interface layup [±45°] corresponding to the eigenvalue $\mathrm{Re}(\lambda_m) - 1 = -0.0642$.

expected for this pure cross-ply interface layup. The displacements in the x-direction are found to exhibit layerwise opposing trends: while in the 0°-layer negative displacements u_x occur, positive displacements are found in the 90°-layer. This deformation mode is clearly a result of the severe mismatch of the elastic properties of the two adjacent plies and as a consequence will lead to inplane normal stresses σ_{xx} in order to balance the differing contraction behaviour of the 0°-ply and the 90°-layer. Furthermore, the present deformation mode is the cause of significant shear strains γ_{xz} and thus, due to Hooke's generalized law (15), also of interlaminar shear stresses σ_{xz}. Furthermore, due to the occurrence of interlaminar shear stresses σ_{xz} the interlaminar normal stress σ_{zz}, which is actually dominated by the computed stress singularity in the vicinity of the free corner, must arise as well which clearly proves the possible criticality of the present free cross-ply laminate corner situation with respect to interlaminar failure like e.g. delamination fracture. The deformation eigenmode for the angle-ply corner $[\pm 45°]$ corresponding to the eigenvalue $\mathrm{Re}(\lambda_m) - 1 = -0.0642$ exhibits a point symmetry with respect to the x-axis: while for u_x the relation $u_x(x,y,z) = u_x(x,-y,-z)$ holds, for u_y and u_z we may state $u_y(x,y,z) = -u_y(x,-y,-z)$ and $u_z(x,y,z) = -u_z(x,-y,-z)$. Due to the differing inplane shear properties of the adjacent $+45°$ and $-45°$-layer, significant inplane shear strains γ_{xy} as well as transverse shear strains γ_{yz} occur, which is also a well established experience when considering stress concentrations at straight free edges in angle-ply laminates. This strain state is responsible for the emergence of inplane shear stresses σ_{xy} and furthermore singular interlaminar shear stresses σ_{yz} so that the presently considered angle-ply layup $[\pm 45°]$ may also be marked as a possibly endangered corner situation which may be prone to corresponding interlaminar failure modes.

3.4.4. 3D stress singularities at interface corners of angle-ply laminates with arbitrary corner opening angles

Beside the investigation of rectangular free corners it is of bacis interest to gain an insight into the asymptotic behaviour of the state variables in the vicinity of free laminate corners with arbitrary opening angles in the range of $0° < \gamma \leqslant 360°$ (see Fig. 14). This situation includes the above discussed situations of free rectangular corners and straight free edges as special cases. As long as the corner opening angle is limited to the interval $0° < \gamma \leqslant 180°$, the meshing strategy remains the same as described in Section 3.4.3: a BFEM mesh on the unit sphere section Γ at $r = 1$ with 112 8-noded elements, 369 nodes, and 1107 degrees of freedom and a variable angle Γ is applied, wherein local mesh refinements are again employed around the two points $r = 1$, $\varphi_1 = 90°$, $\varphi_2 = 0$ and $r = 1$, $\varphi_1 = 90°$, $\varphi_2 = \gamma$ where the two free interface edges intersect with the BFEM surface mesh. The situation changes significantly, however, when the corner opening angle exceeds $\gamma = 180°$, since in this geometric situation the interface corner transforms into a layered notch. This situation involves further stress singularities due to the geometric discontinuity introduced by the structural line at $x = y = 0$ along the z-axis which indeed is the vertex of a three-dimensional layered notch. Hence, for angles $\gamma > 180°$ we have applied further mesh refinements in the vicinity of the two points $x = y = 0$, $z = 1$ and $x = y = 0$, $z = -1$ where the notch vertex intersects with the BFEM mesh in order to adequately capture additional singular influences which of course means a higher computational effort for such corner geometries. Consequently, for all angles $\gamma > 180°$ the BFEM mesh on the unit sphere section Γ at $r = 1$ consists of 280 8-noded surface elements with 905 nodes and 2715 degrees of freedom in all (see Fig. 23 where as an example the

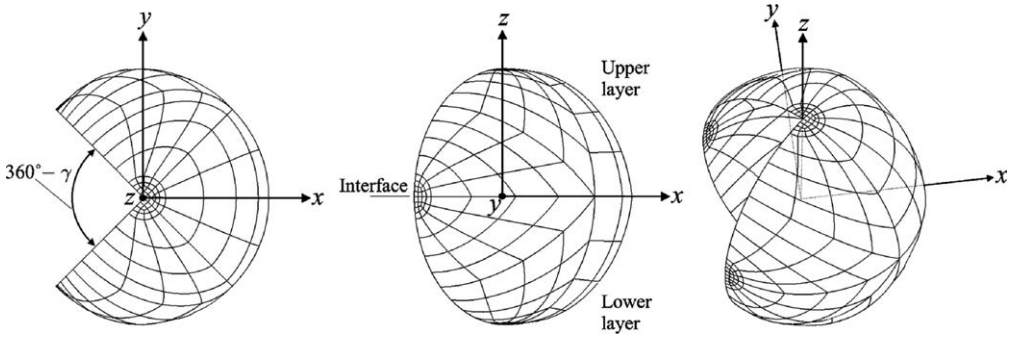

Fig. 23. Locally refined BFEM mesh for a free interface corner with the opening angle $\gamma = 270°$ of a laminate consisting of orthotropic layers with arbitrary inplane material orientations.

BFEM mesh for $\gamma = 270°$ is given) which has again proven to be a reasonable compromise between the achievable accuracy of the results and the needed computational expenses.

As a first step let us investigate the quality of the present BFEM results when compared to the results of e.g. Dimitrov et al. (2002) who have presented numerical results for the orders of the stress singularities at the tip of laminate corners with variable opening angles. Results for the angle-ply interface layup $[\pm 45°]$ are given in Fig. 24, and evidently, an excellent agreement between the results of Dimitrov et al. (2002) and the present BFEM computations is found, lending credibility to our computations. In the interval $0° < \gamma \leqslant 180°$ there occurs only one relevant purely real eigenvalue which is of weak order in comparison to e.g. the classical $r^{-\frac{1}{2}}$-crack tip singularity. For corner opening angles $\gamma > 180°$, two additional relevant eigenvalues emerge which increase in strength for higher angles Γ. At approximately $\gamma = 270°$ a fourth relevant eigenvalue arises, and a maximum absolute value $|\mathrm{Re}(\lambda_m) - 1|$ is encountered at about $\gamma = 330°$ which is even slightly above the classical $r^{-\frac{1}{2}}$-crack tip singularity. For $\gamma = 360°$ (which corresponds to a three-dimensional crack through the thickness of the laminated plate) triple eigenvalues occur which describe the classical $r^{-\frac{1}{2}}$-crack tip singularity.

As a further parameter study we have investigated the orders of the stress singularities at free interface corners with the angle-ply layups $[\pm\theta]$ and with arbitrary corner angles $0° < \gamma \leqslant 360°$, wherein we have considered the material orientation angles $\theta = 15°$, $\theta = 30°$, $\theta = 45°$, $\theta = 60°$, and $\theta = 75°$. The qualitative behaviour of the resultant eigenvalues with varying corner opening angles is similar to the case of the interface layup $[\pm 45°]$ as described above. In all cases there occurs one weak eigenvalue (denoted as $\mathrm{Re}(\lambda_m) - 1 = \lambda_1$, see Fig. 25, upper left portion) which emerges for all considered corner angles Γ except in the case of the $[\pm 75°]$-layup, where seemingly for corner angles of approximately $\gamma < 70°$ no stress singularities occur, which is a remarkable and somewhat unexpected result. An overall minimum value of λ_1 is found for the $[\pm 30°]$-interface at about $\gamma = 54°$. Furthermore, for all considered layups another eigenvalue $\mathrm{Re}(\lambda_m) - 1 = \lambda_2$ emerges at $\gamma = 180°$ (see Fig. 25, upper right portion) which rises monotonously with increasing corner angle Γ, until at $\gamma = 360°$ the classical crack tip stress singularity $r^{-\frac{1}{2}}$ occurs. It is a remarkable outcome that λ_2 is the same for all considered layups (which was also found by Dimitrov et al., 2002), so that this eigenvalue can be interpreted as a characteristic quantity which is governed by the geometry of the structure rather than by the interface layup. A third eigenvalue $\mathrm{Re}(\lambda_m) - 1 = \lambda_3$, which also arises for corner opening angles $\gamma > 180°$ (see Fig. 25, lower left portion), shows a steeper slope than the eigenvalue λ_2 and becomes more pronounced for higher degrees of mismatch of the inplane shear properties of the adjacent layers, i.e. for higher material orientation angles θ. For certain value ranges of Γ, the occurring eigenvalues λ_3 again even slightly exceed the classical crack tip stress singularity $r^{-\frac{1}{2}}$, until at $\gamma = 360°$ the eigenvalue $\mathrm{Re}(\lambda_m) - 1 = -0.5$ again is approximately attained for all layup cases. A fourth eigenvalue $\mathrm{Re}(\lambda_m) - 1 = \lambda_4$ emerges at higher angles Γ which, depending on the laminate layup, are found in the range of about $240° < \gamma < 290°$ (see Fig. 25, lower right portion). The corner angle Γ at which λ_4 emerges becomes smaller for higher material orientation angles θ of the angle-ply layups so that it can be concluded that this eigenvalue is distinctly governed by the layer orientations of the considered laminate layups.

It is of basic interest to discuss the displacement eigenmodes corresponding to those eigenvalues which cause singular stresses in the vicinity of the singularity center. As an important example let us investigate

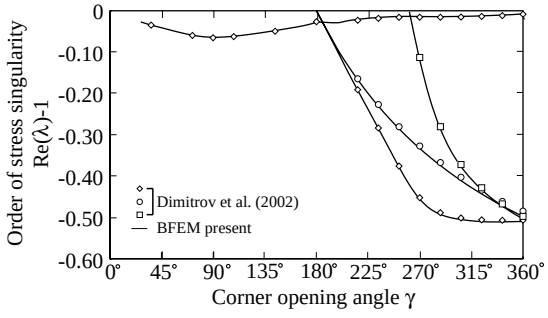

Fig. 24. Three-dimensional stress singularities at a $[\pm 45°]$-interface at the tip of a free laminate corner with arbitrary opening angle γ.

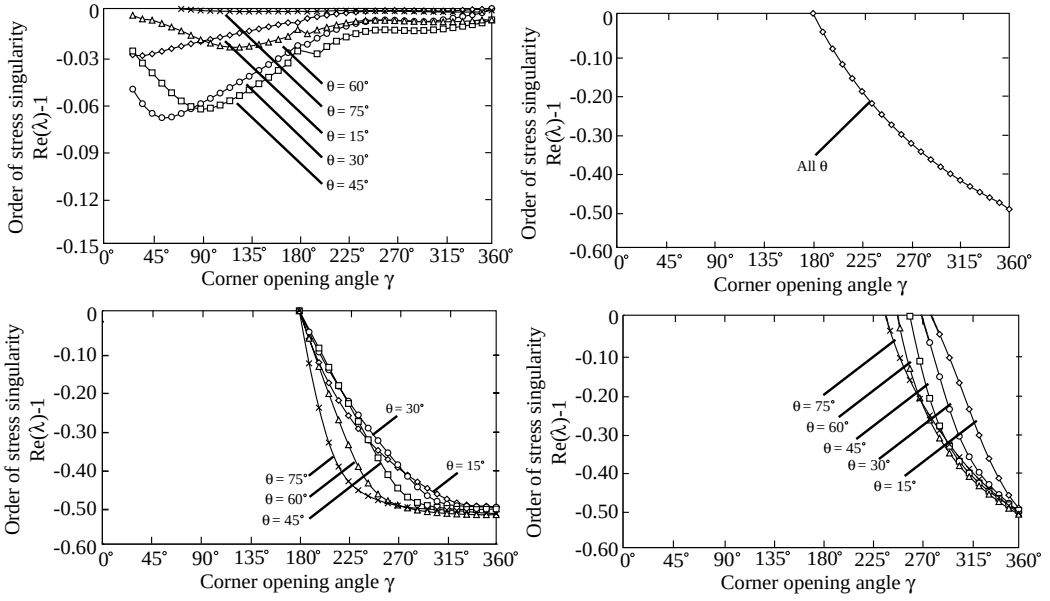

Fig. 25. Three-dimensional stress singularities at $[\pm\theta]$-interfaces at the tip of free laminate corners with arbitrary opening angles γ, eigenvalues λ_1 (upper left portion), λ_2 (upper right portion), λ_3 (lower left portion) and λ_4 (lower right portion).

the deformation modes associated with the dominating eigenvalues λ_2, λ_3 and λ_4 as they are occurring at a free laminate corner with the opening angle $\gamma = 270°$ and the angle-ply interface layup $[\pm 45°]$. The corresponding eigenmodes for the eigenvalues $\lambda_2 = -0.3331$ (denoted as eigenmode 2), $\lambda_3 = -0.4559$ (eigenmode 3) and $\lambda_4 = -0.1188$ (eigenmode 4) are depicted in Fig. 26. It is a somewhat astonishing result that eigenmode 2 is a purely transverse displacement mode (similar to the classical mode III), i.e. only significant out-of-plane displacements u_z occur which explains why the eigenvalue λ_2 is the same for all considered angle-ply layups $[\pm\theta]$: note that such a displacement mode is only governed by the geometry of the laminate corner rather than by the inplane variation of the layerwise fiber orientations in the xy-plane. This is in accord with the conclusions drawn in Dimitrov et al. (2002). Hence, it can be concluded that the eigenvalue λ_2 and the corresponding eigenmode 2 will always be the same for any arbitrary non-orthotropic layup $[\theta_1/\theta_2]$ of the same layer material. The displacement eigenmode 3 exhibits a point symmetry with respect to the x-axis, i.e. we have the relations $u_x(x,y,z) = u_x(x,-y,-z)$ as well as $u_y(x,y,z) = -u_y(x,-y,-z)$ and $u_z(x,y,z) = -u_z(x,-y,-z)$. Beside transverse corner opening displacements (corresponding to the classical out-of-plane mode III), inplane deformations corresponding to the classical deformation mode I which cause an opening of the corner geometry in the xy-plane can also be observed. The remaining displacement eigenmode 4 is found to exhibit the symmetry properties $u_x(x,y,z) = -u_x(x,-y,-z)$ as well as $u_y(x,y,z) = u_y(x,-y,-z)$ and $u_z(x,y,z) = u_z(x,-y,-z)$ and shows characteristics which can be described as a combination of the three classical displacement modes I, II and III: beside a pure corner opening displacement mode (which is similar to the classical mode I) and a pure out-of-plane mode (corresponding to the classical mode III) especially an inplane shearing mode is observed which can be associated with the classical deformation mode II and which is clearly dominating the present displacement eigenmode.

In all, the discussion of the eigenvalues and eigenfunctions which characterize the asymptotic behaviour of the state variables in the vicinity of three-dimensional laminate interface corners reveals that such structural situations pose a challenging and possibly critical problem class in the design and engineering of layered structural elements. It should be noted that there is still a significant backlog in the scientific effort for the understanding of such three-dimensional problems in laminate elasticity, especially when compared to the overwhelming number of publications on simple free-edge effects in laminated strips or other quasi two-dimensional laminate problems.

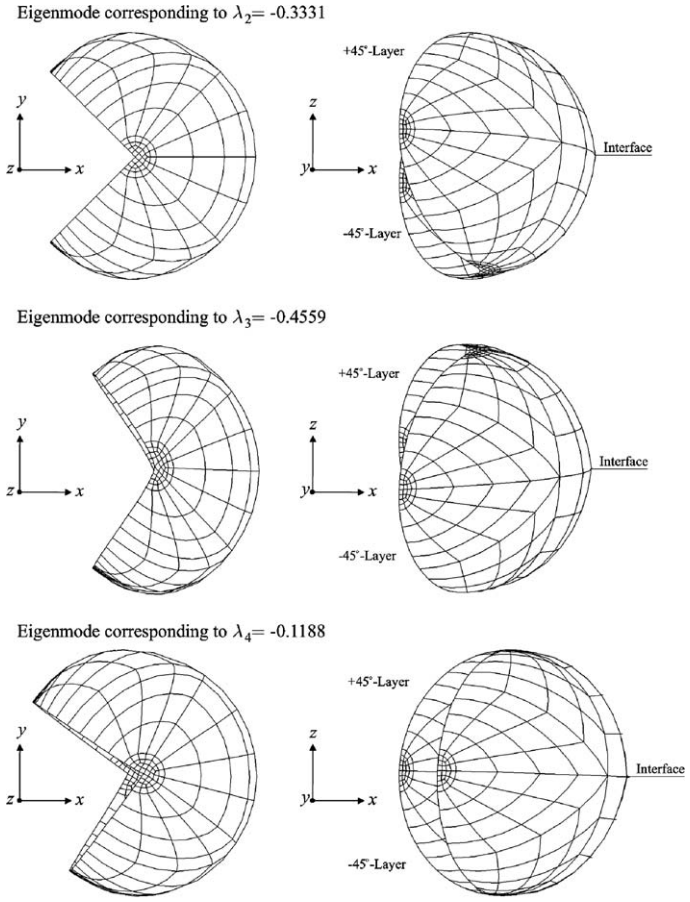

Fig. 26. Displacement eigenmodes for a free interface corner with the opening angle $\gamma = 270°$ of a laminate with the interface layup $[\pm 45°]$ corresponding to the eigenvalues λ_2, λ_3 and λ_4.

4. Summary and conclusions

We have presented numerous results for the orders and modes of stress singularities in the framework of the theory of linear elasticity for several two-dimensional and three-dimensional singular problems like the near fields at the vertices of notches and cracks in homogeneous isotropic halfspaces as well as examples in the framework of laminate elasticity like free-edge effects and free-corner effects in layered plates which are also known to yield significant stress singularities. The computations were performed by the Boundary Finite Element Method (BFEM) which in essence is a semi-analytical fundamental-solution-less boundary element method solely relying on standard finite element formulations. After a throrough literature review on the historical developments in the field of free-edge effects and the application of the BFEM to several problem fields, the theoretical background of the BFEM has been outlined in a concise manner. The application of the BFEM to the engineering problem fields described above has been the focal point of the present contribution. Recapitulating, we may state the following essential conclusions:

- The BFEM is a valuable tool for the analysis of elasticity problems, especially in the presence of stress singularities where standard displacement based finite element methods are known to require huge computational effort and sometimes to even produce questionable results.
- An excellent conformity of the present BFEM results with the results of well-known two-dimensional and three-dimensional benchmark examples has been found, which lends credibility to the BFEM computations. The BFEM has also proven to be advantageous for the computation of the orders and modes of

stress singularities at free laminate edges and, as a more sophisticated and superordinated problem, also at free laminate corners with arbitrary corner opening angles.

- The results for rectangular corners of laminate interfaces between two dissimilar isotropic layers reveal that in such situations significant stress singularities may occur, which decisively depend on the degree of mismatch between the elastic material properties of the adjacent layers.
- The orders of the stress singularities at free rectangular interface corners of laminates consisting of orthotropic layers of e.g. fiber reinforced plastics generally are higher than those occurring at straight free edges of the same layup. However, when compared to classical problems like the stress singularities at the vertices of cracks or also to the results at laminate corners with highly different adjacent isotropic layers, the corner stress singularities in laminates of orthotropic layers are found to be of rather weak order. Nevertheless, free laminate corners pose a problem with involved stress singularities which should also be taken into account in the design and analysis of layered plates like it has long been recognized for free-edge effects.
- At interface corners with opening angles of more than 180°, the corner situation transforms into a layered three-dimensional notch so that in addition to the stress singularities which are induced by the presence of the laminate interface corner there also occur stress singularities due to the effect of the three-dimensional notch geometry. The resultant orders of the stress singularities are characterized by several simultaneous real eigenvalues which in general are very pronounced in comparison with free-corner effects at interface corners with opening angles of less than 180°. In some cases the classical crack tip stress singularity $r^{-\frac{1}{2}}$ is even slightly exceeded, revealing the probable criticality of such structures.

Acknowledgements

The authors are very grateful for the financial support of the DFG—Deutsche Forschungsgemeinschaft—under grant BE-1090/13-1.

References

Abramov, A.A., 1961. On the transfer of boundary conditions for systems of ordinary linear differential equations. Zhurnal Vychislitel'noi Matematiki i Matematicheskoi Fiziki 1, 542–545.

Altus, E., Rotem, A., Shmueli, M., 1980. Free edge effect in angle ply laminates—a new three dimensional finite difference solution. Journal of Composite Materials 14, 21–30.

Artel, J., Becker, W., in press. Coupled and uncoupled analysis of piezoelectric free-edge effect in laminated plates. Composite Structures.

Barsoum, R.S., 1990. Asymptotic fields at interfaces using the finite element iterative method. Computers and Structures 35, 285–292.

Bauld, N.R., Goree, J.G., Tzeng, L.-S., 1985. A comparison of finite-difference and finite-element methods for calculating free edge stresses in composites. Computers and Structures 20, 897–914.

Bazant, Z.P., Keer, L.M., 1974. Singularities of elastic stresses and of harmonic functions at conical notches or inclusions. International Journal of Solids and Structures 10, 957–964.

Bazant, Z.P., Estenssoro, L.F., 1979. Surface singularity and crack propagation. International Journal of Solids and Structures 15, 405–426.

Becker, W., 1993. Closed-form solution for the free-edge effect in cross-ply laminates. Composite Structures 26, 39–45.

Becker, W., 1994. Closed-form analysis of the free edge effect in angle-ply laminates. Journal of Applied Mechanics 61, 209–211.

Becker, W., Jin, P.P., Neuser, P., 1999. Interlaminar stresses at the free corners of a laminate. Composite Structures 45, 155–162.

Bellman, R., Kagiwada, H., Kalaba, R., 1967. Invariant embedding and the numerical integration of boundary-value problems for unstable linear systems of ordinary differential equations. Communications of the ACM 10, 100–102.

Benthem, J.P., 1977. State of stress at the vertex of a quarter-infinite crack in a half-space. International Journal of Solids and Structures 13, 479–492.

Benthem, J.P., 1980. The quarter-infinite crack in a half-space; alternative and additional solutions. International Journal of Solids and Structures 16, 119–130.

Bossavit, A., Fremond, M., 1976. The frontal method based on mechanics and dynamic programming. Computer Methods in Applied Mechanics and Engineering 8, 153–178.

Bui, H.D., 1994. Inverse Problems in the Mechanics of Materials: An Introduction. CRC Press, Boca Raton.

Cho, M., Kim, H.S., 2000. Iterative free-edge stress analysis of composite laminates under extension, bending, twisting and thermal loadings. International Journal of Solids and Structures 37, 435–459.

Dasgupta, G., 1982. A finite element formulation for unbounded homogeneous continua. Journal of Applied Mechanics 49, 136–140.

Davi, G., 1996. Stress fields in general composite laminates. AIAA Journal 34, 2604–2608.

Deeks, A.J., Wolf, J.P., 2002a. Stress recovery and error estimation for the scaled boundary finite-element method. International Journal for Numerical Methods in Engineering 54, 557–583.

Deeks, A.J., Wolf, J.P., 2002b. An h-hierarchical adaptive procedure for the scaled boundary finite-element method. International Journal for Numerical Methods in Engineering 54, 585–605.

Deeks, A.J., Wolf, J.P., 2002c. A virtual work derivation of the scaled boundary finite-element method for elastostatics. Computational Mechanics 28, 489–504.

Delale, F., 1984. Stress singularities in bonded anisotropic materials. International Journal of Solids and Structures 20, 31–40.

Dimitrov, A., Andrae, H., Schnack, E., 2001. Efficient computation of order and mode of corner singularities in 3D-elasticity. International Journal for Numerical Methods in Engineering 51, 1–24.

Dimitrov, A., Andrae, H., Schnack, E., 2002. Singularities near three-dimensional corners in composite laminates. International Journal of Fracture 115, 361–375.

Ding, S., Kumosa, M., 1994. Singular stress behaviour at an adhesive interface corner. Engineering Fracture Mechanics 47, 503–519.

Gaudenzi, P., Mannini, A., Carbonaro, R., 1998. Multi-layer higher-order finite elements for the analysis of free-edge stresses in composite laminates. International Journal for Numerical Methods in Engineering 41, 851–873.

Griffin, O.H., 1988. Three-dimensional thermal stresses in angle-ply composite laminates. Journal of Composite Materials 22, 53–70.

Gruttmann, F., Wagner, W., 1994. On the numerical analysis of local effects in composite structures. Composite Structures 29, 1–12.

Gu, L., Belytschko, T., 1994. A numerical study of stress singularities in a two-material wedge. International Journal of Solids and Structures 31, 865–889.

Haskell, N.A., 1964. Radiation pattern of surface waves from point sources in a multi-layered medium. Bulletin of the Seismological Society of America 54, 377–393.

Herakovich, C.T., Post, D., Buczek, M.B., Czarnek, R., 1985. Free edge strain concentrations in real composite laminates: experimental-theoretical correlation. Journal of Applied Mechanics 52, 787–793.

Herakovich, C.T., 1989a. Free edge effects in laminated composites. Handbook of Composites, Vol. 2. Elsevier Science Publishers B.V., Amsterdam, pp. 187–230.

Herakovich, C.T., 1989b. Failure modes and damage accumulation in laminated composites with free edges. Composites Science and Technology 36, 105–119.

Herakovich, C.T., 1998. Mechanics of Fibrous Composites. John Wiley & Sons, Inc., New York.

Herrmann, K.P., Linnenbrock, K., 2002. Three-dimensional thermal crack growth in self-stressed bimaterial joints: analysis and experiment. International Journal of Fracture 114, 133–151.

Hsu, P.W., Herakovich, C.T., 1977. Edge effects in angle-ply composite laminates. Journal of Composite Materials 11, 422–428.

Icardi, U., Bertetto, A.M., 1995. An evaluation of the influence of geometry and of material properties at free edges and at corners of composite laminates. Computers and Structures 57, 555–571.

Isakson, G., Levy, A., 1971. Finite-element analysis of interlaminar shear in fibrous composites. Journal of Composite Materials 5, 273–276.

Kant, T., Swaminathan, K., 2000. Estimation of transverse/interlaminar stresses in laminated composites—a selective review and survey of current developments. Composite Structures 49, 65–75.

Kassapoglou, C., Lagace, P.A., 1986. An efficient method for the calculation of interlaminar stresses in composite materials. Journal of Applied Mechanics 53, 744–750.

Kim, R.Y., 1989. Experimental observations of free-edge delamination. Composite Materials Series, Vol. 5. Elsevier, Amsterdam, pp. 111–160.

Kim, T., Atluri, S.N., 1994. Interlaminar stresses in composite laminates under out-of-plane shear/bending. AIAA Journal 32, 1700–1708.

Kim, T.W., Im, S., 1995a. Boundary layers in wedges of laminated composite strips under generalized plane deformation—part I: asymptotic solutions. International Journal of Solids and Structures 32, 609–628.

Kim, T.W., Im, S., 1995b. Boundary layers in wedges of laminated composite strips under generalized plane deformation—part II: complete numerical solutions. International Journal of Solids and Structures 32, 629–645.

Koguchi, H., 1997. Stress singularity analysis in three-dimensional bonded structure. International Journal of Solids and Structures 34, 461–480.

Krishna Murty, A.V., Hari Kumar, H.K., 1989. Modelling of symmetric laminates under extension. Composite Structures 11, 15–32.

Labossiere, P.E.W., Dunn, M.L., 2001. Fracture initiation at three-dimensional bimaterial interface corners. Journal of the Mechanics and Physics of Solids 49, 609–634.

Lessard, L.B., Schmidt, A.S., Shokrieh, M.M., 1996. Three-dimensional stress analysis of free-edge effects in a simple composite cross-ply plate. International Journal of Solids and Structures 33, 2243–2259.

Li, J., Zhang, X.-B., Recho, N., 2001. Stress singularities near the tip of a two-dimensional notch formed from several elastic anisotropic materials. International Journal of Fracture 107, 379–395.

Li, J., Recho, N., 2002. Methode asymptotique en mecanique de la rupture. Hermes-Lavoisier, Paris.

Li, J., 2002. Singularity analysis of near-tip fields for notches formed from several anisotropic plates under bending. International Journal of Solids and Structures 39, 5767–5785.

Lindemann, J., Becker, W., 2000. Analysis of the free-edge effect in composite laminates by the boundary finite element method. Mechanics of Composite Materials 36, 355–366.

Lindemann, J., Becker, W., 2002a. The tendency for free-edge delamination in laminates and its minimization. Composites Science and Technology 62, 233–242.

Lindemann, J., Becker, W., 2002b. Free-edge stresses around holes in laminates by the boundary finite-element method. Mechanics of Composite Materials 38, 407–416.
Mannini, A., Gaudenzi, P., 2003. Multi-layer higher-order finite elements for the analysis of free-edge stresses in piezoelectric actuated laminates. Composite Structures 61, 271–278.
Mittelstedt, C., Becker, W., 2003a. Three-dimensional closed-form analysis of the stress field at rectangular corners of layered plates. Archive of Applied Mechanics 73, 63–74.
Mittelstedt, C., Becker, W., 2003b. Free-corner effects in cross-ply laminates: an approximate higher-order theory solution. Journal of Composite Materials 37, 2043–2068.
Mittelstedt, C., Becker, W., 2004a. Interlaminar stress concentrations in layered structures—part I: a selective literature survey on the free-edge effect since 1967. Journal of Composite Materials 38, 1037–1062.
Mittelstedt, C., Becker, W., 2004b. Interlaminar stress concentrations in layered structures—part II: closed-form analysis of stresses at laminated rectangular wedges with arbitrary non-orthotropic layup. Journal of Composite Materials 38, 1063–1090.
Mittelstedt, C., Becker, W., 2004c. Thermoelastic fields in boundary layers of isotropic laminates. Journal of Applied Mechanics 72, 86–101.
Mittelstedt, C., Becker, W., 2004d. A variational finite layer technique for the analytical investigation of free-corner effects in composite structures. Journal of Thermal Stresses 27, 953–981.
Müller, A., Hohe, J., Becker, W., 2002. A closed-form analysis of material and geometry effects on stress singularities at unsymmetric bimaterial notches. In: Proceedings of the 73rd GAMM—Gesellschaft für Angewandte Mathematik und Mechanik - Annual Meeting. Augsburg, Germany.
Müller, A., Wenck, J., Goswami, S., Lindemann, J., Hohe, J., Becker, W., in press. The boundary finite element method for predicting directions of cracks emerging from notches at bimaterial junctions. Engineering Fracture Mechanics.
Öry, H., Reimerdes, H.-G., Dieker, S., 1984. Berechnung von interlaminaren Spannungen in mehrschichtigen Faserverbundwerkstoffen mit Hilfe von Übertragungsmatrizen. Zeitschrift für Flugwissenschaften und Weltraumforschung 8, 392–404.
Pagano, N.J., 1974. On the calculation of interlaminar normal stress in composite laminate. Journal of Composite Materials 8, 65–81.
Pagano, N.J., 1978a. Stress fields in composite laminates. International Journal of Solids and Structures 14, 385–400.
Pagano, N.J., 1978b. Free edge stress fields in composite laminates. International Journal of Solids and Structures 14, 401–406.
Picu, C.R., Gupta, V., 1997. Three-dimensional stress singularities at the tip of a grain triple junction line intersecting the free surface. Journal of the Mechanics and Physics of Solids 45, 1495–1520.
Pipes, R.B., Pagano, N.J., 1970. Interlaminar stresses in composite laminates under uniform axial extension. Journal of Composite Materials 4, 538–548.
Pipes, R.B., Daniel, I.M., 1971. Moire analysis of the interlaminar shear edge effect in laminated composites. Journal of Composite Materials 5, 255–259.
Pipes, R.B., Pagano, N.J., 1974. Interlaminar stresses in composite laminates—an approximate elasticity solution. Journal of Applied Mechanics 41, 668–672.
Pipes, R.B., 1980. Boundary layer effects in composite laminates. Fibre Science and Technology 13, 49–71.
Prasanna Rajan, V.S., Raju, K.C.J., 2002a. Theoretical aspects of a novel scaled boundary finite element formulation in computational electromagnetics. http://arxiv.org/ftp/physics/papers/0210/0210077.pdf (August 4th, 2004).
Prasanna Rajan, V.S., Raju, K.C.J., 2002b. Constraint relations between the unknown coefficients in the scaled boundary finite element formulation in electromagnetics. http://arxiv.org/ftp/physics/papers/0210/0210078.pdf (August 4th, 2004).
Puppo, A.H., Evensen, H.A., 1970. Interlaminar shear in laminated composites under generalized plane stress. Journal of Composite Materials 4, 204–220.
Raju, I.S., Crews, J.H., 1981. Interlaminar stress singularities at a straight free edge in composite laminates. Computers and Structures 14, 21–28.
Reddy, J.N., 2004. Mechanics of Laminated Composite Plates and Shells, second ed. CRC Press, Boca Raton.
Robbins Jr., D.H., Reddy, J.N., 1996. Variable kinematic modelling of laminated composite plates. International Journal for Numerical Methods in Engineering 39, 2283–2317.
Rohwer, K., 1982. On the determination of edge stresses in layered composites. Nuclear Engineering and Design 70, 57–65.
Rose, C.A., Herakovich, C.T., 1993. An approximate solution for interlaminar stresses in composite laminates. Composites Engineering 3, 271–285.
Rybicki, E.F., 1971. Approximate three-dimensional solutions for symmetric laminates under inplane loading. Journal of Composite Materials 5, 354–360.
Seweryn, A., Molski, K., 1996. Elastic stress singularities and corresponding generalized stress intensity factors for angular corners under various boundary conditions. Engineering Fracture Mechanics 55, 529–556.
Somaratna, N., Ting, T.C.T., 1986. Three-dimensional stress singularities in anisotropic materials and composites. International Journal of Engineering Science 24, 1115–1134.
Song, C., Wolf, J.P., 1995a. Consistent infinitesimal finite-element-cell method: out-of-plane motion. Journal of Engineering Mechanics 121, 613–619.
Song, C., Wolf, J.P., 1995b. Consistent infinitesimal finite-element-cell method: three-dimensional vector wave equation. International Journal for Numerical Methods in Engineering 39, 2189–2208.
Song, C., Wolf, J.P., 1996. Consistent infinitesimal finite-element cell method for diffusion equation in unbounded medium. Computer Methods in Applied Mechanics and Engineering 132, 319–334.

Song, C., Wolf, J.P., 1997. The scaled boundary finite-element method—alias consistent infinitesimal finite-element cell method—for elastodynamics. Computer Methods in Applied Mechanics and Engineering 147, 329–355.

Song, C., Wolf, J.P., 1998a. The scaled boundary finite-element method for anisotropic multimaterial plate with crack. In: Proceedings International Symposium on Boundary Element Methods (IABEM 98). Paris, France.

Song, C., Wolf, J.P., 1998b. The scaled boundary finite-element method: analytical solution in frequency domain. Computer Methods in Applied Mechanics and Engineering 164, 249–264.

Song, C., Wolf, J.P., 1999a. The scaled boundary finite element method—alias consistent infinitesimal finite element cell method—for diffusion. International Journal for Numerical Methods in Engineering 45, 1403–1431.

Song, C., Wolf, J.P., 1999b. Body loads in scaled boundary finite-element method. Computer Methods in Applied Mechanics and Engineering 180, 117–135.

Song, C., Wolf, J.P., 2000. The scaled boundary finite-element method—a primer: solution procedures. Computers and Structures 78, 211–225.

Song, C., Wolf, J.P., 2001a. Semi-analytical evaluation of dynamic stress-intensity factors. In: Proceedings First Asian-Pacific Congress on Computational Mechanics. Sydney, Australia.

Song, C., Wolf, J.P., 2001b. The scaled boundary finite-element method—a fundamental solution-less boundary-element method. Computer Methods in Applied Mechanics and Engineering 190, 5551–5568.

Song, C., Wolf, J.P., 2002. Semi-analytical representation of stress singularities as occurring in cracks in anisotropic multi-materials with the scaled boundary finite-element method. Computers and Structures 80, 183–197.

Spilker, R.L., 1980. A traction-free-edge hybrid-stress element for the analysis of edge effects in cross-ply laminates. Computers and Structures 12, 167–179.

Spilker, R.L., Chou, S.C., 1980. Edge effects in symmetric composite laminates: importance of satisfying the traction free edge condition. Journal of Composite Materials 14, 2–20.

Stolarski, H.K., Chiang, M.Y.M., 1989. On the significance of the logarithmic term in the free edge stress singularity of composite laminates. International Journal of Solids and Structures 25, 75–93.

Tahani, M., Nosier, A., 2003. Free edge stress analysis of general cross-ply composite laminates under extension and thermal loading. Composite Structures 60, 91–103.

Tang, S., 1975. A boundary layer theory—part I: laminated composites in plane stress. Journal of Composite Materials 9, 33–41.

Ting, T.C.T., Chou, S.C., 1981. Edge singularities in anisotropic composites. International Journal of Solids and Structures 17, 1057–1068.

Wang, A.S.D., Crossman, F.W., 1977. Some new results on edge effect in symmetric composite laminates. Journal of Composite Materials 11, 92–106.

Wang, S.S., Choi, I., 1982a. Boundary-layer effects in composite laminates, part 1: free-edge stress singularities. Journal of Applied Mechanics 49, 541–548.

Wang, S.S., Choi, I., 1982b. Boundary-layer effects in composite laminates, part 2: free-edge stress solutions and basic characteristics. Journal of Applied Mechanics 49, 549–560.

Wang, S.S., Yuan, F.G., 1983a. A singular hybrid finite element analysis of boundary-layer stresses in composite laminates. International Journal of Solids and Structures 19, 825–837.

Wang, S.S., Yuan, F.G., 1983b. A hybrid finite element approach to composite laminate elasticity problems with singularities. Journal of Applied Mechanics 50, 835–844.

Whitcomb, J.D., Raju, I.S., Goree, J.G., 1982. Reliability of the finite element method for calculating free edge stresses in composite laminates. Computers and Structures 15, 23–37.

Whitcomb, J.D., Raju, I.S., 1983. Superposition method for analysis of free-edge stresses. Journal of Composite Materials 17, 492–507.

Whitney, J.M., Browning, C.E., 1972. Free-edge delamination of tensile coupons. Journal of Composite Materials 6, 300–303.

Whitney, J.M., 1989. Experimental characterization of delamination fracture. Composite Materials Series, Vol. 5. Elsevier, Amsterdam, pp. 161–250.

Wigger, H.M., Becker, W., 2004. Characterization of inplane loaded anisotropic interface corners with the boundary finite element method. Computational Mechanics, submitted paper.

Wolf, J.P., Song, C., 1995. Consistent infinitesimal finite-element-cell method: in-plane motion. Computer Methods in Applied Mechanics and Engineering 123, 355–370.

Wolf, J.P., Song, C., 1996a. Finite-element Modelling of Unbounded Media. John Wiley & Sons, Chichester.

Wolf, J.P., Song, C., 1996b. Consistent infinitesimal finite element cell method: three-dimensional scalar wave equation. Journal of Applied Mechanics 63, 650–654.

Wolf, J.P., Song, C., 1998a. The scaled boundary finite-element method—a fundamental-solution-less boundary element method. In: Proceedings of the Fourth World Congress on Computational Mechanics. Buenos Aires, Argentina.

Wolf, J.P., Song, C., 1998b. Unit-impulse response of unbounded medium by scaled boundary finite-element method. Computer Methods in Applied Mechanics and Engineering 159, 355–367.

Wolf, J.P., Song, C., 2000. The scaled boundary finite-element method—a primer: derivations. Computers and Structures 78, 191–210.

Wolf, J.P., Song, C., 2002. The semi-analytical fundamental-solution-less scaled boundary finite-element method to model unbounded soil. In: Proceedings Euromech Colloquium 414, Boundary Element Methods for Soil/Structure Interaction. Catania, Italy.

Wolf, J.P., 2003. The Scaled Boundary Finite Element Method. John Wiley & Sons, Chichester.

Wu, C.M.L., 1987. Nonlinear analysis of edge effects in angle-ply laminates. Computers and Structures 25, 787–798.

Yamada, Y., Okumara, H., 1981. Analysis of local stress in composite materials by the 3D finite element. In: Composite Materials: Proceedings of the Japan–U.S. Conference. Tokyo, Japan.

Ye, L., 1990. Some characteristics of distributions of free-edge interlaminar stresses in composite laminates. International Journal of Solids and Structures 26, 331–351.

Yeh, J.R., Tadjbakhsh, I.G., 1986. Stress singularity in composite laminates by finite element method. Journal of Composite Materials 20, 347–364.

Yin, W.-L., 1994. Free-edge effects in anisotropic laminates under extension, bending and twisting, part I: a stress-function-based variational approach. Journal of Applied Mechanics 61, 410–415.

Zhong, W.X., 1994. Plane elasticity in sectorial domain and the Hamiltonian system. Applied Mathematics and Mechanics 15, 1113–1123.

Zhu, C., Lam, Y.C., 1998. A Rayleigh-Ritz solution for local stresses in composite laminates. Composites Science and Technology 58, 447–461.

Zwiers, R.I., Ting, T.C.T., Spilker, R.L., 1982. On the logarithmic singularity of free-edge stress in laminated composites under uniform extension. Journal of Applied Mechanics 49, 561–569.